Parting ways – removal of salts and organic micropollutants by direct nanofiltration

Pretreatment of surface water for the production of dune infiltration water

Suzanne van der Poel

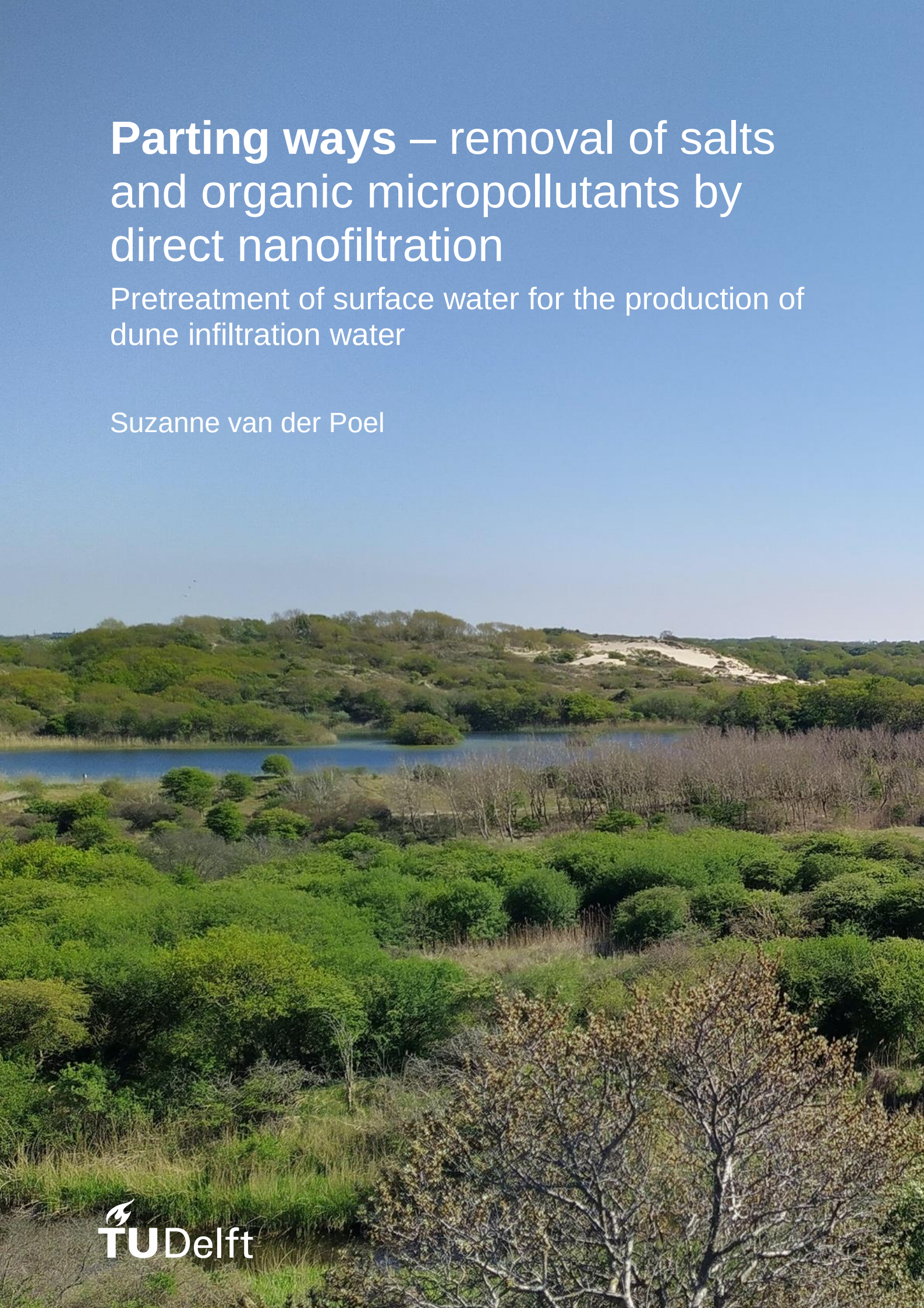

TU Delft

Parting ways – removal of salts and organic micropollutants by direct nanofiltration

Pretreatment of surface water for the production of dune infiltration water

By

Suzanne van der Poel, MA

in partial fulfilment of the requirements for the degree of

Master of Science (MSc)
in Civil Engineering

at Delft University of Technology,
to be defended publicly on Monday 14 December 2020 at 15:00 PM.

Supervisor:	Dr. ir. S.G.J. (Bas) Heijman,	TU Delft
Thesis committee:	Prof. dr. ir. L.C. (Luuk) Rietveld,	TU Delft
	Dr. T.J. (Tom) Savenije,	TU Delft
	Dr. ir. F.C. (Franca) Kramer,	Dunea

An electronic version of this thesis is available at http://repository.tudelft.nl/.

Acknowledgements

Omdat het zo persoonlijk is, schrijf ik mijn dankwoord in de taal waarin ik mij het beste uit kan drukken. Na een studie Nederlands en een aantal omzwervingen besloot ik in 2014 mijn grenzen verder te verleggen en aan de opleiding Civiele Techniek te beginnen in Delft. Mijn studiepad ligt niet het meest voor de hand maar het heeft precies zo moeten zijn – als een rivier die zijn eigen weg baant. Af en toe was het een wilde rit, maar ik ben dankbaar dat ik mij op twee zulke verschillende gebieden heb mogen ontwikkelen. En nu, ruim zes jaar later is het zover: ik studeer bijna af en neem daarmee afscheid als student aan de TU Delft. Daarom ook symbolisch: *parting ways*. De rivier mondt bijna uit op open water, een zee aan mogelijkheden voor de boeg.

Een hoop mensen verdienen een woord van dank, maar ik begin bij mijn begeleiders. Franca, ik ben blij dat je me onder je hoede hebt genomen bij Dunea en gedurende het hele proces van afstuderen voor me klaarstond. Je bent een heel betrokken begeleider. Mijn dank is groot! Bedankt Bas, voor je begeleiding en altijd praktische oplossingen, zelfs vanaf afstand. Luuk, jouw enthousiasme heeft me voor drinkwaterzuivering doen kiezen, dank hiervoor en natuurlijk ook voor je feedback. Tom, met jouw chemische achtergrond bracht je een welkome andere blik op mijn afstudeerproject. Bedankt daarvoor. Doris, je bent voor mij een grote inspiratiebron. Dank dat je mijn rolmodel wilt zijn.

Dank ook aan het team van Bron tot Kraan, Clemy in het bijzonder, die mij samen met Franca geholpen heeft om een bijna professioneel waterlabje op pompstation Scheveningen te creëren. Armand, Patricia en Jane, bedankt voor jullie ondersteuning in het Waterlab. Dank aan Luc en Tineke van Het Waterlaboratorium voor het meedenken en de analyses. Anurag, Roberto and Erik, thanks for all the support from NX Filtration. Roos, bedankt voor je positiviteit en je ondersteuning.

Marleen, vriendin vanaf dag een, jouw nuchtere blik helpt mij relativeren. Eline, na onze onafscheidelijke jaren op de middelbare school ben ik blij dat we ook een aantal jaar in Delft hebben kunnen delen. Bedankt voor jullie vriendschappen. Maarten: dank voor je wijze raad, onze gesprekken zijn van grote waarde voor me.

Papa, mama, jullie hebben me altijd gesteund om door te gaan en gemotiveerd om het meeste uit mijzelf te halen. Dank voor jullie onvoorwaardelijke steun en vertrouwen. Lisette, je bent niet alleen mijn zusje maar ook een van mijn beste vriendinnen met wie ik alles kan delen. De afgelopen maanden heb je me de afleiding gegeven die ik nodig had. Tot slot, lieve Sjoerd, mijn rots in de branding, dank voor alles en alles. Met jou durf ik alles aan wat komen gaat.

Suzanne van der Poel

Den Haag, december 2020

Abstract

New techniques are urgently demanded to remove organic micropollutants (OMPs) such as endocrine disrupting compounds, pharmaceuticals and pesticides from our drinking water sources. With increasing salinity of surface waters in coastal regions, salt removal has also become an issue in the production of drinking water. When advanced oxidation processes are combined they are capable to remove OMPs to a large extent, but without the removal of salts. Dense membranes like reverse osmosis (RO) or flat-sheet nanofiltration (NF) membranes – which require an extensive pretreatment – can sufficiently remove OMPs and salts, but only at low permeabilities and by producing a saline waste stream. Hollow fiber NF membranes seem very promising in this respect as they have higher permeabilities, lower energy consumptions and can be applied directly. In this study, the removal of salts and OMPs from synthetic surface water and real lake water from the Valkenburgse Meer (VM) by the polyelectrolyte multilayer (PEM) coated dNF40 membrane was studied in order to make it suitable for dune infiltration water. This type of membrane is fabricated by depositing polycations and polyanions alternately on a porous support medium, also known as the layer by layer (LbL) technique, which enables control of the membrane's surface charge and permeability. Hollow fiber NF membranes have the ability to separate ions or solutes with smaller sizes and hydraulic radii than the pore size of the membrane due to electrostatic repulsion. The membrane is negatively charged at neutral pH.

The dNF40 membrane showed ion retentions of up to 27% for Cl^-, 98% for SO_4^{2-}, 87% for Mg^{2+}, 76% for Ca^{2+} and 17% for Na^+ in once-through configuration with a hydraulic permeability of 5.8 $Lm^{-2}h^{-1}$ and molecular weight cut-off (MWCO) of ~200 Da. However, lower ion retention values were observed for filtration of real lake water, except for SO_4^{2-}. Retentions were unaffected by cross-flow velocity, but increased with increasing permeate flux. Moreover, the ion retentions reduced considerably when the system recovery increased to 75%. In addition to the salt retentions, the retention of a mix of 20 distinctively different pharmaceuticals, both positively charged, negatively charged and neutral OMPs with molecular weights between 119 and 748 $gmol^{-1}$, was investigated. An average retention as high as 79% and 89% was reached for SW (no natural organic matter (NOM)) and VM water (11.6 mgL^{-1} of NOM), respectively. As expected, the negatively charged pharmaceuticals were retained best as a result of electrostatic interactions with the negatively charged membrane, followed by the positively charged compounds, of which repulsion is probably promoted by underlying polycation layers in the membrane structure. Neutral compounds were retained less.

The dNF40 membrane showed to be resistant to fouling, while no extensive pretreatment was applied, making it suitable for direct treatment of surface water. Furthermore, OMPs were largely removed, hardness was partially reduced and NOM was almost completely removed, but insufficient NaCl was retained to meet dune infiltration water standards. Therefore, an additional step becomes necessary in the pretreatment of surface water. Four suggestions were provided.

Contents

Abstract v
Nomenclature viii
Abbreviations x
List of figures xi
List of tables xiii
Introduction 1
1.1 Background: production of drinking water by Dunea 1
1.2 Problem statement 2
1.3 Research question and objectives 3
Literature review 5
2.1 Occurrence of OMPs in Dutch surface water 5
2.2 Treatment technologies for the production of infiltration water from surface water 6
2.2.1 Advanced oxidation of pre-treated surface water 6
2.2.2 Membrane filtration of pre-treated surface water 8
2.2.2.1 NF with spiral wound membranes 8
2.2.2.2 RO 10
2.2.3 Direct NF of surface water with hollow fiber LbL membranes 11
2.3 Configuration and structure of polyelectrolyte NF membranes 13
2.4 Transport mechanism – the Nernst Planck Model 15
2.5 Retention mechanisms 15
2.5.1 Steric rejection: the ‘sieve effect’ 15
2.5.2 Donnan exclusion: the repulsion effect 16
2.5.3 Solute-membrane affinity 17
2.6 Operational parameters 17
2.6.1 pH and temperature 17
2.6.2 Feed composition 17
2.6.3 Cross-flow velocity 17
2.6.4 Permeate flux 18
2.6.2 Hydraulic pressure loss 18
2.6.3 (System) recovery 18
2.7 Fouling mechanisms 19
2.7.1 (Bio)fouling 19
2.7.2 Scaling 20
Materials and methods 21
3.1 Experimental set-up 21
3.2 Filtration experiments 23

3.2.1 Hydraulic permeability 24
3.2.2 Molecular weight cut-off 24
3.2.3 Filtration with SW 25
3.2.4 Filtration with VM water 26
3.2.5 Cleaning the membranes 26
3.3 Sampling 26
3.4 Composition of the water 28
3.4.1 Water matrices of Dunea tap water, SW and VM water 28
3.4.2 Selection of OMPs 28
3.5 Physical and chemical analysis 30
Results and discussion 31
4.1 Hydraulic permeability 31
4.2 Molecular weight cut-off 32
4.3 Influence of Cl^- concentration on Cl^- retention 33
4.4 Effect of cross-flow velocity on ion retention 33
4.5 Influence of permeate flux on ion retention 35
4.6 Influence of system recovery on ion retention 36
4.7 Performance towards OMPs 38
4.8 Comparison of effluent at 75% system recovery with requirements for infiltration water 43
Conceptual design 45
5.1 A full-scale dNF40 plant for pretreatment location Katwijk 45
5.2 Visual impressions of the dNF plant 46
5.3 Elaboration of the scenarios 49
5.3.1 Side stream RO 49
5.3.2 Mixing with Meuse water 51
Conclusion 53
Recommendations 55
Bibliography 57
Appendix: Control tests MWCO 64
Appendix: Retention OMPs 65
Appendix: Conceptual design 66

Nomenclature

μ	dynamic viscosity	[Pa.s]
$\boldsymbol{\rho}$	density of a fluid	[kgm^{-3}]
$\boldsymbol{\psi}$	electrical potential	[mV]
$\boldsymbol{\Delta\pi}$	osmotic pressure difference across the membrane	[Pa]
$\boldsymbol{\gamma}$	recovery	[%]
$\boldsymbol{\lambda}$	friction factor	[-]
$\boldsymbol{\sigma}$	reflection coefficient	[-]
$\boldsymbol{c_i}$	concentration of a solute *i*	[M]
$\boldsymbol{A_{cross-section}}$	cross-sectional area of a single fiber	[m^2]
$\boldsymbol{A_{filtration}}$	active filtration area	[m^2]
$\boldsymbol{D_i^{\infty}}$	solute diffusion coefficient at infinite dilution	[m^2s^{-1}]
$\boldsymbol{d}$	diameter of a pipe	[m]
$\boldsymbol{d_{inner}}$	inner diameter of a fiber	[m]
$\boldsymbol{d_s}$	pore diameter	[nm]
$\boldsymbol{F}$	Faraday's constant	[96485.33 $Cmol^{-1}$]
$\boldsymbol{H}$	hydraulic head	[m]
$\boldsymbol{J_i}$	solute flux	[$Lm^{-2}h^{-1}$]
$\boldsymbol{J_w}$	water flux	[$Lm^{-2}h^{-1}$]
$\boldsymbol{K_{i,c}}$	convective hindrance parameter	[-]
$\boldsymbol{K_{i,d}}$	diffusive hindrance parameter	[-]
$\boldsymbol{K_w}$	water permeability of the membrane	[m]
$\boldsymbol{l}$	length of a fiber	[m]
$\boldsymbol{L}$	length of a pipe	[m]
$\boldsymbol{L_{21°C}}$	temperature-corrected permeability	[$Lm^{-2}h^{-1}bar^{-1}$]
$\boldsymbol{\log D}$	pH corrected octanol-water partitioning coefficient	[-]
$\boldsymbol{\log K_{OW}}$	octanol-water partitioning coefficient	[-]
$\boldsymbol{MW}$	molecular weight	[Da]
$\boldsymbol{n}$	number of fibers in a module	[-]
$\boldsymbol{pKa}$	acid dissociation constant	[-]
$\boldsymbol{\Delta P}$	transmembrane pressure	[bar]
$\boldsymbol{\Delta P_H}$	hydraulic pressure loss	[bar]
$\boldsymbol{q_{feed}}$	feed flow	[m^3s^{-1}]
$\boldsymbol{q_{permeate}}$	permeate flow	[m^3s^{-1}]
$\boldsymbol{q_{concentrate}}$	concentrate flow	[m^3s^{-1}]
$\boldsymbol{Q}$	flow through a pipe	[m^3s^{-1}]

$\boldsymbol{R_g}$	universal gas constant	[8.314 $JK^{-1}mol^{-1}$]
$\boldsymbol{R_i}$	retention of a solute *i*	[%]
$\boldsymbol{S_{MW}}$	standard deviation of the molecular weight distribution	[Da]
$\boldsymbol{T}$	temperature	[°C]
$\boldsymbol{v_{cf}}$	cross-flow velocity	[ms^{-1}]
$\boldsymbol{V_f}$	feed volume	[m^3]
$\boldsymbol{V_p}$	permeate volume	[m^3]
$\boldsymbol{x}$	distance	[m]
$\boldsymbol{z_i}$	charge of a solute *i*	[-]

Abbreviations

AMPA	aminomethylphosphonic acid
AOP	advanced oxidation process
CF	concentration factor
CP	concentration polarization
cfv	cross-flow velocity
dNF	direct nanofiltration
DWTP	drinking water treatment plant
DOC	dissolved organic carbon
EC	electrical conductivity
HPLC	high-performance liquid chromatography
LbL	layer by layer
MWCO	molecular weight cut-off
NF	nanofiltration
NOM	natural organic matter
OMP	organic micropollutant
PAA	poly(acrylic acid), polyanion
PAC	powdered activated carbon
PAH	poly(allylamine hydrochloride), polycation
PDADMAC	poly(diallyldimethylammonium chloride), polycation
PDF	process flow diagram
PEG	polyethylene glycol
PEM	polyelectrolyte multilayer
PES	polyethersulfone
PSBMA	poly N-(3-sulfopropyl)-N-(methacryloxyethyl)-N,N-dimethylammonium betaine, polyzwitterion
PSS	poly(sodium 4-styrenesulfonate), polyanion
RO	reverse osmosis
RSF	rapid sand filtration
SSF	slow sand filtration
SW	synthetic water
TFC	thin-film composite
TMP	transmembrane pressure
TOC	total organic carbon
VM	Valkenburgse Meer

List of figures

Figure 1. Dead-end and cross-flow filtration modes. Adapted from Wang et al. (2011) 13
Figure 2. Schematic of feed flow through a hollow fiber NF membrane unit. Source: https://filtsol.com/main/index.php/technical-info/hollow-fiber-membranes. 13
Figure 3. Fabrication of polyelectrolyte multilayers (PEMs) with alternating deposition of polycation (PDADMAC) and polyanion (PSS) on the polyamide NF membrane (NFG). Source: Cheng et al. (2018) 14
Figure 4. Representation of the Donnan equilibrium, where the concentration of co-ions is lower at the membrane surface than in the solution, while the concentration of counter-ions is higher. 16
Figure 5. P&ID MexPlorer lab scale installation NX Filtration 21
Figure 6. Sampling schedule of feed (F1-2) and permeate (P1-3) during each experiment with recycling 26
Figure 7. Sampling schedule of feed (F1-4), permeate (P1-3) and mixed permeate (P_{mix}1-3) during recovery experiments. 27
Figure 8. Clean water flux at different TMPs (cfv= 0.6 ms^{-1}; T=20ºC). 31
Figure 9. Determination of the molecular weight cut-off (MWCO) of the dNF40 membrane by filtration of PEG molecules (J=18 $Lm^{-2}h^{-1}$; cfv=0.6 ms^{-1}; T= 21°C). 32
Figure 10. Retention of Cl^- (left) during increasing concentration in the feed and permeate concentrations (right) during dNF (cfv=0.6 ms^{-1}; J=18 $Lm^{-2}h^{-1}$; T=21°C). 33
Figure 11. Retention of different ions during dNF of SW containing ~120 mgL^{-1} Cl^- (J=18 $Lm^{-2}h^{-1}$; T=21°C). 34
Figure 12. Retention of different ions during dNF of SW with ~120 mgL^{-1} Cl^- and VM water with ~230 mgL^{-1} Cl^- at varying permeate fluxes (cfv= 0.6 ms^{-1}; T=21°C). 35
Figure 13. Cl^- concentration of the feed (crosses), permeate (triangles) and mixed permeate (dots) at different system recoveries during filtration of SW (left) and VM water (right) (J=18 $Lm^{-2}h^{-1}$; cfv=0.6 ms^{-1}; T=21°C). The concentration factor (CF) is shown with respect to the initial Cl^- concentration. 36
Figure 14. Cl^- retention with increasing system recovery during filtration of SW (left) and VM water (right). Retention (triangles) computed by concentration in permeate with respect to the concentration in the feed tank and average retention (dots) by concentration in mixed permeate with respect to the initial concentration. 37
Figure 15. Retention of different ions during filtration of SW (blue) and VM water (green) at 25%, 50% and 75% system recovery (J=18 $Lm^{-2}h^{-1}$; cfv=0.6 ms^{-1}; T=21°C). 38
Figure 16. Rejection of selected pharmaceuticals in synthetic and real surface water at pH 8. 39
Figure 17. Deviating retention of six OMPs by the dNF40 membrane as a function of molecular weight and feed water type. 41
Figure 18. Visual impression of a single dNF stage with 84 modules within one treatment lane, preceded by three 100-micron strainers. 47

Figure 19. Visual impression of a treatment lane consisting of three stages, where the concentrate of the first stage continues as feed water for the second stage. All produced permeate is collected separately. 47
Figure 20. Overview of the dNF plant Katwijk with 12 treatment lanes for the treatment of 32 million m^3y^{-1} from the VM. 48
Figure 21. Location of the dNF40 plant in Katwijk. 48
Figure 22. Process flow diagram (PFD) and hydraulic line of dNF plant with side stream RO treatment. 50
Figure 23. Different ion concentrations in infiltration water originating from the Meuse and in the abstracted water after dune passage. Data from Het Waterlaboratorium obtained by Dunea. 51
Figure 24. MWCO control test by filtration of 200 Da PEG molecules (J=18 $Lm^{-2}h^{-1}$; cfv=0.6 ms^{-1}; T=21°C). 64
Figure 25. MWCO control test by filtration of 300 Da PEG molecules (J=18 $Lm^{-2}h^{-1}$; cfv=0.6 ms^{-1}; T=21°C). 64
Figure 26. Retention of different OMPs during filtration of SW after 24h and 48h and VM water (cfv=0.6 ms^{-1}; T=21°C). Labels of rejection values <90% are shown. 65
Figure 27. Transport pipeline from the VM to treatment location Katwijk (left) and transport pipeline for concentrate disposal from Katwijk to the North Sea (right). Adapted from Kraaijeveld et al. (2020) 66

List of tables

Table 1. Legend P&ID MexPlorer (Figure 4) 22
Table 2. Specifications of the dNF40 lab scale membrane module, provided by the supplier 23
Table 3. Experimental conditions 23
Table 4. Water composition of Dunea tap water (data from 18 August 2020), SW (with 3 different NaCl concentrations) and VM water. Some ions could not be detected (<d.l.) as their concentrations were very low. 28
Table 5. Physico-chemical characteristics of the selected OMPs. 29
Table 6. Structure and physico-chemical characteristics of six deviating OMPs. 42
Table 7. Comparison of parameters of interest of SW and VM water at 75% system recovery with requirements for infiltration water. The values of Dunea and legal standards are the maximum desired and allowed values. Values exceeding the maxima of the legal standard are indicated in red. 43
Table 8. Average Cl^- concentrations from 2016-2020 in the VM. 44
Table 9. Comparison of the designs of a full-scale dNF plant for Katwijk operating at 75% and 85% system recovery in summer and winter period based on the projection tool. 45
Table 10. Concentrations in mgL^{-1} of various ions in two mixing scenarios together with the expected Ca^{2+} concentration and hardness in $mmolL^{-1}$ after dune passage. 52
Table 11. Summer and winter water quality of the VM used for the projections. 66

1 Introduction

1.1 Background: production of drinking water by Dunea

Dutch drinking water company Dunea uses the dunes, amongst others, as a natural barrier against pathogens. As recharge in the dunes by rain water is not sufficient to supply fresh water to 1.3 million customers in the province of Zuid-Holland, river water is infiltrated artificially into the dunes. Surface water from the river Meuse (primary source) or sometimes Lek (secondary source) is taken in and stored in a side branch for approximately six weeks. In order to remove phosphate and improve settling of suspended solids (SS), iron sulfate ($FeSO_4$) is dosed. Micro strainers are used during spring and summer to remove algae and larvae. This step ensures the protection of the transport pipelines. The water is transported to the pretreatment location at Bergambacht, where rapid sand filtration (RSF) takes place. The water is then transported through a pipeline of over 80 km long to the western part of the Netherlands and infiltrated into three different dune areas. After a retention time of about two months, the water is abstracted and used for the production of drinking water at the post-treatment locations of Katwijk, Scheveningen and Monster (Knol et al., 2015; Zwolsman, 2019).

The quality of the river water has significantly decreased in the past years and the large transportation distance is found to be vulnerable (Zwolsman, 2019). Therefore, Dunea started to investigate the possibility of treating water locally, nearby the production locations. A third source is also desired to meet the water demand that keeps increasing due to the increasing population in the Randstad – an agglomeration of cities in the western part of the Netherlands. Close to the city of Leiden, a large fresh water lake is located: the Valkenburgse Meer (VM) where 32 million m^3y^{-1} could be taken in, which would fulfill the needs of the entire production location of Katwijk. The lake is located only 5 km away from the infiltration area Berkheide.

In terms of quality, the VM already has a relatively low SS content which is comparable to the Afgedamde Maas after $FeSO_4$ dosing, although chloride (Cl^-) , phosphate (PO_4^{3-}), dissolved organic carbon (DOC) and SS concentrations should be reduced before infiltration to protect the vulnerable dune valleys (Zwolsman, 2019). Organic micropollutants (OMPs) are also a point of concern. Elevated levels of aminomethylphosphonic acid (AMPA), a degradation product of the broadly applied pesticide glyphosate (WHO, 2003), have for example been detected (Zwolsman, 2019). Therefore, there is a challenge to implement an appropriate technique for treating VM water in order to meet infiltration water standards.

1.2 Problem statement

In Europe, millions of people depend on surface waters such as the rivers Rhine and Meuse for their need of drinking water (Houtman, 2010). However, in the past years, the availability and quality of river water has decreased. Prolonged droughts cause decreasing river discharges, resulting in an increase in salt and pollutants concentration. In addition, seawater intrusion in fresh water sources becomes an increasing problem in coastal areas (Zwolsman, 2019). The occurrence of micropollutants such as hormones, pesticides, pharmaceuticals and personal care products in drinking water sources has raised public concern in the last decades (Sanches et al., 2012). Growing welfare and world population lead to increased levels of micropollutants in surface and drinking water sources, threatening both the aquatic environment and drinking water quality (Te Brinke et al., 2020a).

Pesticides are widely applied in agriculture to protect crops from pathogens, insects and weeds. Active components of these pesticides enter surface waters by agriculture runoff or leach into groundwater (Sjerps et al., 2019). Their occurrence in Dutch ground- and surface water sources used for drinking water production has been determined as well. In one third of the abstraction areas in The Netherlands, pesticide and/or metabolites concentration exceeded water quality standards according to the Water Framework Directive (Sjerps et al., 2019). In addition, pharmaceuticals have been detected in the aquatic environment, mainly due to the emission of sewage water treatment plant effluent on surface water (Houtman et al., 2014). Elimination of pesticides, pharmaceuticals, fuel additives, flame-retardants, plasticizers and numerous other industrial pollutants by conventional wastewater and drinking water processes has not been shown to be effective (Acero et al., 2010). Consequently, there is a need to investigate advanced technologies for their removal.

Advanced oxidation and membrane filtration are the two emerging technologies to reduce concentrations of OMPs in pretreated surface water (Knol et al., 2015), since the most common technology, i.e. adsorption, does not sufficiently reduce OMPs concentrations from waste- and surface water streams as it can remove OMPs up to ~90% (Te Brinke et al., 2020a). Membrane technologies are more promising in this regard because they can reach higher retentions (Te Brinke et al., 2020a). Membrane filtration is a separation process where the membrane acts as a ‘selective barrier’ (Mulder, 2012). The two types of pressure-driven membrane filtration used for OMP removal in drinking water production are nanofiltration (NF) and reverse osmosis (RO) (Wang et al., 2011). RO showed an OMP removal of >90%, but is an energy-consuming technique due to its low water permeability (Te Brinke et al., 2020a), though energy consumption is also depended on the salt concentration of the feed water. Commercially available NF membranes are less energy intensive. However, their increased permeability has resulted in lower retentions than with RO (Verliefde et al., 2008).

Nevertheless, in the last 30 years, NF has been described as very efficient for the removal of natural organic matter (NOM), hardness, bacteria, viruses, salinity, nutrients such as nitrates and phosphates, and OMPs such as pesticides and pharmaceuticals (Verberk et al., 2002; Van der Bruggen & Vandecasteele, 2003; Sanches et al., 2012). NF membranes are also promoted as an attractive

alternative to lime softening in conventional groundwater treatment (Van der Bruggen & Vandecasteele, 2003; Wang et al., 2011).

In NF installations, spiral wound membranes are most commonly applied (Verberk et al., 2002). They have a large specific area, resulting in low investment costs, but the disadvantage is the requirement of an extensive pretreatment as they have a high tendency for fouling (Verberk et al., 2002). This makes spiral wound membranes less suitable for direct treatment of surface water with a high suspended solids content. Capillary NF membranes, or hollow fiber membranes, have been designed to reduce membrane fouling (Van der Bruggen et al., 2003). Their biggest advantage is the possibility to treat (surface) water almost directly, with minimal pretreatment of feed water. Often only preceded cartridge filtration is necessary. This treatment is also known as direct NF (dNF), where the need of several steps used in conventional drinking water treatment such as coagulation, flocculation and sand filtration are eliminated. Furthermore, capillary NF membranes are easy to clean, and have a higher permeability, leading to lower operating pressure and a correspondingly lower energy consumption (Van der Bruggen et al., 2003).

The drawback of NF is the production of a (highly) saline concentrate stream (Abtahi et al., 2018). Novel NF membranes where layer-by-layer (LbL) technique is applied, make it possible to achieve high OMP rejection with partial salt retention depending on the assembly of polyelectrolyte multilayers (PEMs) (Abtahi et al., 2018; Reurink et al., 2018; Te Brinke et al., 2020a). A rejection as high as 98% towards a common mix of OMPs has been reached, with a retention of only 10-15% NaCl (Te Brinke et al., 2020a). Monovalent salt retention could be improved by a different assembly of the PEMs, leading to NaCl retentions above 50% together with 98% OMP removal, while remaining high permeability (Te Brinke et al., 2020b). Retentions are not only dependent on PEM selection but also on the conditions during the coating process (Te Brinke et al., 2020b). There are various mechanisms that play a role in the removal of OMPs. Mechanisms such as size exclusion and hydrophobic interactions were found to highly influence the obtained rejections (Sanches et al., 2012). Electrostatic interactions also have an effect on the rejection of (charged) OMPs (Verliefde et al., 2008; Hajibabania et al., 2011). However, the removal mechanisms due to this LbL structure are yet fully to be understood.

1.3 Research question and objectives

Although a rising number of papers are published on LbL NF and its capacity to remove OMPs, most of them are based on a OMP cocktail in pure water or with a single salt added (Reurink et al., 2019; Te Brinke et al., 2020a). However, real water is much more complex and can influence retentions of both ions and OMPs (Devitt et al., 1998; Sanches et al., 2012). Treatment of surface water specifically with LbL NF membranes has not been reported in literature. This research focuses on filtration of surface water to gain more insight in the performance of this type of membrane in combination with a complex water matrix. Synthetic water (SW), where the composition of lake water was simulated, was filtrated and next to that, real water from the Valkenburgse Meer was tested as case-study. Furthermore, many of the 20 selected OMPs studied in this research have not been tested before with LbL NF membranes.

Thus, the overall objective of this study is to assess the performance of the LbL dNF40 membrane for direct surface water treatment and obtain insight in the retention of various ions in a complex water matrix and the rejection mechanism of OMPs, to make it suitable for dune infiltration. The aim is to answer the following research questions.

1. To what extent does the LbL dNF40 membrane remove salts and OMPs from surface water?
2. What effects do feed concentration, cross-flow velocity, permeate flux and system recovery have on the retention of ions in a surface water matrix during filtration with the LbL dNF40 membrane?

The specific objectives of this study are:

(i) Comparing emerging technologies for OMP and salt removal from surface water for the production of dune infiltration water.

(ii) Assessing the treatment performance of LbL NF membranes in different water matrices: synthetic surface water and real surface (lake) water from the Valkenburgse Meer.

(iii) Gaining insight in the removal mechanisms of OMPs. What effect has the LbL structure of the membrane on the removal of OMPs?

(iv) Verifying if the water produced with dNF of surface water meets the standards of dune infiltration water.

(v) Designing a robust full-scale dNF40 plant for the infiltration site of Berkheide.

2

Literature review

2.1 Occurrence of OMPs in Dutch surface water

The occurrence of OMPs in ground- and surface waters has become an important concern for the drinking water industry (Verliefde et al., 2007a). OMPs, also called emerging contaminants, cover a broad range of synthetic chemicals e.g. pesticides, pharmaceuticals, drugs, personal and household care products, cosmetics, and industrial chemicals such as perfluorinated compounds and flame retardants, which are essential to modern human society (Houtman et al., 2010; Ilyas et al., 2017). Large amounts of very diverse pharmaceuticals are produced worldwide, and their activity at very low concentrations (in the range of nanograms per liter) has made occurrence of pharmaceuticals in the aquatic environment problematic. For example, endocrine disrupting compounds (EDCs) such as hormones can have a disturbing effect on the hormonal system. The synthetic hormone 17α-ethinylestradiol has been reported to cause feminization in male fish at concentrations as low as 1 ng/L (Verliefde et al., 2007a). In the past decade, increasing concern has risen on GenX and other perfluorinated compounds (PFAS) that have been widely used for the production of stain- and water-resistant coatings, which are toxic and difficult to remove from water by traditional treatment (Beekman et al., 2016; Hopkins et al., 2018). Some OMPs, including perfluorooctanoic acid (PFOA), are capable of bioaccumulation in organisms, posing a potential risk to human health (Reemtsma et al., 2016).

The emission of domestic wastewater treatment plant effluent on surface waters has been identified as a major source of pharmaceuticals in the environment (Houtman et al., 2014). Wastewater treatment plants have generally not been designed to remove such compounds, and therefore they can be found in drinking water sources (Wols et al., 2013). Moreover, direct industrial discharges affect surface water quality across Europe because not all chemicals are removed by industrial wastewater treatment plants (Van Wezel et al., 2018). This is public concern in a country like The Netherlands as 40% of the produced drinking water is prepared from surface water, predominantly from of the rivers Rhine and Meuse (Houtman et al., 2014). Houtman et al. (2014) calculated lifelong exposure to (a mixture of) pharmaceuticals via drinking water to be extremely low. However, concentrations are expected to rise in the future: climate change and thus more frequent and severe low river discharges leads to periods with increased concentrations of synthetic chemicals in our surface water (Van Wezel et al., 2018). Newly introduced chemicals also can have a different cocktail effect, so caution is advised. To prevent OMPs ending up in our dunes and eventually in our drinking water, efficient OMP removal in our drinking water treatment facilities is thus of greatest importance.

OMPs are small sized – they have a molecular weight of 100-1000 Da –, which makes it difficult to be removed by conventional treatment (Te Brinke et al., 2020a). Removal efficiency is furthermore influenced by the charge of the pollutant and its hydrophobicity. The charge of the solute is determined by the pK_a value of the solute. The hydrophobicity, or polarity, of a compound can be expressed by the octanol-water partitioning coefficient (log K_{OW}). The higher the log K_{OW} value (>2), the more hydrophobic (i.e. apolar) a compound. Polar or hydrophilic compounds (log K_{OW} < 2) are difficult to be removed by traditional water treatment so that they often slip through (Verliefde et al., 2007a; Reemtsma et al., 2016). Often the log *D* value is considered as a better indicator for hydrophobicity, as this parameter takes the pH of the water matrix into account (Tetko & Bruneau, 2004; Abtahi et al., 2018):

$$\log D = \log K_{OW} - \log\left(1 + 10^{-|pH - pK_a|}\right)$$

In this regard, compounds with log *D* > 2.6 are considered hydrophobic – they prefer to accumulate in solid phases instead of being soluble in the aqueous phase – and hydrophilic if log *D* ≤ 2.6 (Abtahi et al., 2018).

2.2 Treatment technologies for the production of infiltration water from surface water

The increasing concern about OMPs in drinking water sources in the 1990s has led to a two-track approach to tackle this problem: on the one hand, pressure was exerted by the government on farmers and producers to develop alternatives for the use of pesticides. On the other hand, drinking water barriers were improved by implementing granular or powdered activated carbon (GAC/PAC) filtration (Verliefde et al., 2007a; Brunner et al., 2020), an adsorptive technique which preferentially removes hydrophobic organic solutes (Schoonenberg Kegel et al., 2010). However, complete removal is often not achieved (KWR, 2020). The combination of increasing concentrations of OMPs in surface waters due to growing and aging populations and global warming, and the inadequate removal of polar compounds by the (improved) conventional treatment train, require additional barriers against OMPs (Knol et al., 2015). In this section, several emerging technologies are evaluated that could be implemented for the treatment of surface water to make it suitable for dune infiltration water, based on their removal capacity of OMPs and salts.

2.2.1 Advanced oxidation of pre-treated surface water

Knol et al. (2015) investigated the conversion of OMPs and the formation of bromate by advanced oxidation process (AOP) with O_3/H_2O_2 (peroxone) of pre-treated surface water. The source of this water is a dead-end tributary from the river Meuse, where $FeSO_4$ is dosed to reduce the phosphate concentration. After a residence time of several weeks, the water is extracted and passes 35 µm micro sieves after which it is transported to Bergambacht. Here, the water is further treated by dual media RSF. The pre-treated water was spiked with 14 OMPs with different sensitivities for (direct) oxidation. Compared to other AOP technologies such as UV/H_2O_2, the peroxone process is known as energy

efficient (Knol et al., 2015; Scheideler et al., 2011). However, the disadvantage of AOP is the reaction of ozone with bromide (Br^-) into bromate (BrO_3^-), which is suspected to be carcinogenic (Knol et al., 2015). To comply with a bromate concentration below 0.5 μgL^{-1} – a Dunea guideline, the Dutch drinking water act prescribes a maximum value of 1 μgL^{-1} for bromate –, the optimal dosage was found to be 1.5 mgL^{-1} ozone and 6 mgL^{-1} hydrogen peroxide, leading to an average OMP removal of 78.9%. The two mechanisms behind OMP conversion are direct oxidation by ozone and oxidation by in-situ produces hydroxyl radicals (•OH) (Knol et al., 2015). The addition of hydrogen peroxide accelerates the decomposition of ozone and limits bromate formation (Knol et al., 2015; Bourgin et al., 2017). O_3 and •OH also react with NOM, therefore the water quality matrix influences the efficiency of the peroxone process. Higher water temperatures and lower concentrations of organic matter increased conversion of OMPs (Knol et al., 2015).

The efficiency of peroxone treatment was also studied with Swiss surface water from Lake Zürich, pretreated by ultrafiltration (UF) and spiked with 19 OMPs (Bourgin et al., 2017). All 19 OMPs were reduced by more than 87% at 3 mgL^{-1} ozone and 9 mgL^{-1} hydrogen peroxide, while only 7 compounds were reduced up to this level at 0.5 mgL^{-1} ozone. The fairly limited conversion of some OMPs by peroxone could be explained by the poor ability of these compounds to oxidize by ozone alone. Reactivity of organic compounds towards ozone is strongly dependent on molecular structure (Knol et al., 2015). Ozone mainly attacks on electron rich sites of for example aromatic rings and C=C double bonds. After the AOP, post-treatment with GAC filtration was required to further reduce OMP concentration, remove the transformation products formed during oxidation and the residual O_3 and H_2O_2 (Bourgin et al., 2017). This drawback leads to an extensive treatment train.

Another barrier against OMPs is the UV/H_2O_2 process, where the pollutants are degraded by means of photon attack (direct UV photolysis) and •OH oxidation (Wols et al., 2013). The degradation of a large group of 40 pharmaceuticals by UV/H_2O_2 was studied by Wols et al. (2013). Experiments with water from the river Meuse, among others, were carried out, pre-treated by Dunea in Bergambacht according the aforementioned manner. For natural water types, most of the OMPs were degraded by 90% at UV doses between 500-1000 $mJcm^{-2}$ and 10 mgL^{-1} hydrogen peroxide (Wols et al., 2013). Like peroxone treatment, the efficiency of UV/H_2O_2 depends on sensitivity of the solutes towards UV and hydroxyl radicals. Most OMPs which contain a benzene ring or double C=C bond in the molecular structure required more energy for oxidation (Wols et al., 2013). Furthermore, the presence of HCO_3^- and NOM causes hydroxyl radical scavenging, resulting in a lower OMP oxidation (Wols et al., 2013).

The Dutch surface water companies – Dunea, PWN, Waternet and Evides (DPWE) – assessed three pilot installations, consisting of O_3/H_2O_2-UV/H_2O_2, UV/H_2O_2-GAC and UF-RO, specifically for the removal of OMPs from pre-treated surface water based on target analysis, non-target screening and bioassays (Brenner et al., 2020). All three processes removed most OMPs to a large extent (>80%). The sequential O_3/H_2O_2-UV/H_2O_2 process, which is considered to be implemented after the RSF step in Bergambacht, showed an average OMP removal of 95% (Brunner et al., 2020) and was already priced

as an economically attractive option compared to the separated processes by Scheideler et al. (2011). With 2 gm^{-3} ozone, 6 gm^{-3} hydrogen peroxide and an energy requirement of 0.26 $kWhm^{-3}$ for UV irradiation, the investigated compounds were reduced by >80%, while bromate formation was limited to 1 μgL^{-1} (Scheideler et al., 2011).

For the UV/H_2O_2-GAC pilot plant, water from the IJsselmeer was used, pre-treated with drum sieves, coagulation/sedimentation, rapid sand filters, and activated carbon filtration. Subsequently, the water is transported and infiltrated in the dunes. The extended UV/H_2O_2-GAC shows very good removal as most of the spiked compounds were removed to a large extend (>90%), with exception of 4 persistent OMPs. Transformation products originated from UV/H_2O_2 were for the most part removed by the additional GAC step. Brunner et al. (2020) concluded that there seems to be at least one effective treatment process for almost every OMP, except for melamine. However, none of the investigated processes was able to remove all dosed substances to a large extent. This selectivity results in always requiring a combination of processes, making the already extensive pretreatment even more complex. Additionally, AOPs do not reduce salt concentrations. This combined makes AOP a less attractive option for treatment of VM water as salt reduction is one of the requirements.

2.2.2 Membrane filtration of pre-treated surface water

2.2.2.1 NF with spiral wound membranes

As water treatment processes, NF and RO are often considered as effective remediation techniques for OMPs (Verliefde et al., 2008; Schoonenberg Kegel et al., 2010). NF membranes fall in the transition region between pore-flow and solution-diffusion membranes and typically have a dense separating layer which is more open than a RO membrane (Reurink et al., 2018). The molecular weight cut-off (MWCO, the molar mass above which more than 90% of the compounds is rejected) of NF membranes lies in the range of 200-500 $gmol^{-1}$, corresponding to the molar mass of most of the OMPs present in source waters for drinking water production (Verliefde et al., 2007a). NF membranes can operate with higher fluxes and lower energy requirements than RO membranes (Malaisamy et al., 2011). However, with increasing permeability comes lower retentions, especially toward small and uncharged micropollutants such as bisphenol A (Te Brinke et al., 2020a). Relatively low rejection and selectivity for monovalent ions is also exhibited, as NF rejects less than 60% of monovalent ions (Malaisamy et al., 2011).

Experiments with 9 pharmaceuticals and 5 endocrine disruptors showed an overall rejection of a clean spiral wound polyamide NF-200 membrane (MWCO of 300 Da) of ~63% for hydrophobic and hydrophilic neutral compounds. The NF-90 membrane (MWCO of 200 Da) rejected nearly all hydrophobic neutral compounds (95-98%) and 62-96% of the hydrophilic neutral compounds (Yangali-Quintanilla et al., 2009). However, Verliefde et al. (2007b) experienced a decrease in rejection with increasing solute hydrophobicity for neutral pharmaceuticals with real surface water. Maybe the adsorption equilibrium was not reached yet in the case of Yangali-Quintanilla et al., resulting in an overestimation of rejection. Ionic compounds were mainly rejected by electrostatic repulsion between the negatively charged solutes and a negatively charged membrane surface (71-94% by NF-200 and 99% by NF-90) (Yangali-

Quintanilla et al., 2009). These results are in line with research of Verliefde et al. (2008). They demonstrated that the rejection values for negatively charged pharmaceuticals were the highest, followed by the rejection values for neutral ones. Positively charged pharmaceuticals showed the lowest rejection values (Verliefde et al., 2007b&2008).

Two source waters were used in the research of Verliefde et al. (2007b&2008): the first type is surface water from the intake of a treatment plant in Amsterdam (operated by Waternet). This water was pre-treated with coagulation-flocculation-sedimentation, passage through a reservoir with a residence time of about 100 days, followed by RSF. Rejection values of >75% for all pharmaceuticals with the Desal HL membrane (MWCO 150-300 Da), and even >85% with the Trisep TS-80 membrane (MWCO of 200 Da) were reached when operating at low recovery (10%). The second type is surface water from the river Schie in Delft, pre-treated with a weak acidic cationic exchange resin in order to prevent scaling in the NF unit by exchanging multivalent scaling cations (Ca^{2+}, Mg^{2+} and Si^{4+}) for Na^{+} ions (Verliefde et al., 2007b). To reduce turbidity and remove particles, the water is treated with UF before it is fed to the combined system of NF with subsequent activated carbon filtration. With the NF-GAC set-up, water of almost impeccable quality was produced as >98% of all pharmaceuticals was removed. The high removal was attributed to the fact that less competition occurred between NOM and pharmaceuticals for adsorption onto the GAC, since most of the organic matter is removed in the NF step. However, one major drawback of the robust dual barrier NF-GAC combination is the disposal of the NF concentrate stream.

Sanches et al. (2012) reached 67.4-99.9% removal of different pesticides and hormones from real surface water by NF (membrane MWCO of 150-300 Da), pre-treated with UF to remove particulate and large colloidal organic matter. They found size exclusion and hydrophobic interactions to influence the obtained rejections. The concentration of divalent SO_4^{2-} was reduced with >55.4%, while the Cl^- concentration was only reduced with 26.6 ± 3.8% (Sanches et al., 2012). This higher rejection of divalent ions was also observed by Costa & De Pinho (2006). Rejection of 98, 55 and 64% for $MgSO_4$, NaCl and $CaCl_2$, respectively, were reached with a spiral wound NF membrane with a MWCO of 200 Da (Costa & De Pinho, 2006). However, with NF of real surface water from the river Tagus (Portugal), preceded by 0.45 µm membrane filtration, much higher salt rejection was obtained for NaCl and $CaCl_2$ due to complex formation of cations with humic substances that are retained by the membrane (Costa & De Pinho, 2006). The requirement for electroneutrality caused rejection of anions at the same time.

Negatively charged organic solutes are well retained by spiral wound NF membranes. The overall OMP rejection values are also are promising, but complete removal is not achieved. As the influence of OMPs and their combined effect – even in low concentrations – is yet to be fully understood, high removal is desirable. Therefore, a combined treatment or post-treatment with activated carbon filtration is often required, resulting in a complex process. Moreover, flat sheet membranes are very susceptible to fouling and require an extensive pretreatment (Van der Bruggen et al., 2003), which is costly and has a large footprint.

2.2.2.2 RO

RO is a pressure-driven physical separation process, consisting of membranes based on dense separating layers through which the passage of organic solutes occurs by means of solution-diffusion (Wang et al., 2011; Reurink et al., 2018; Albergamo et al., 2019). Complex interactions between solute and membrane can promote or hinder this solution-diffusion mechanism (Verliefde et al., 2008). RO filtration in itself does not involve chemical reactions, so in contrast to AOPs, by- or transformation products are not expected in the treated water, unless disinfection agents such as chlorine are used, or by (bio)fouling (Albergamo et al., 2019). To prevent fouling of the membranes, an adequate pretreatment is required.

Albergamo et al. (2019) studied the removal of polar OMPs from Dutch surface water by RO treatment. The source water was naturally pre-treated with riverbank filtration – an actual source for a drinking water utility in the province of Zuid-Holland – and the anaerobic filtrate was kept under hypoxic conditions during RO filtration to prevent precipitation of dissolved iron. They found that neutral and moderate hydrophobic OMPs were substantially removed (>95%, except for one target compound). Neutral OMPs are removed by size exclusion while hydrophobic compounds are also influenced by solute-membrane affinity interactions. Neutral hydrophilic OMPs larger than 180 Da were removed for 99%. The smallest OMPs displayed the lowest removal efficiencies. Their passage could be lowered by applying tighter RO membranes or in combination with other treatments (Albergamo et al., 2019). Negatively charged OMPs were removed by >99%, while a small breakthrough of cationic OMPs was observed. In addition to steric hindrance, the excellent removal of negative OMPs is reached by the electrostatic repulsion between anionic solutes and the negatively charged membranes.

Diminished efficiencies for small and hydrophobic (apolar) organic compounds were also obtained by Schoonenberg Kegel et al. (2010). They studied the efficiency of RO treatment for the removal of OMPs from riverbank filtrate by drinking water company Vitens. After riverbank filtration, the water is pre-treated by aeration and RSF to remove the larger particles, iron, manganese and ammonium that can cause fouling to the RO membrane. A split stream of 50% of the pre-treated water is fed to the RO plant with 80% recovery. The RO rejection values for almost all solutes were high (>95%), except for the very small (hydrophilic) compound NDMA (60%), and the small hydrophobic solutes ethylbenzene (9%) and naphthalene (53%). To increase OMP removal, both the bypass water and the RO permeate were finally treated with activated carbon filtration, resulting in removal of a larger part of the studied OMPs (Schoonenberg Kegel et al., 2010).

Of the three investigated installations by DPWE, the UF-RO process showed high average removal of OMPs (most compounds were rejected by >90%, despite a few substances that exhibited removal <60%) (Brunner et al., 2020). The same pre-treated IJsselmeer water was used as in the UV/H_2O_2-GAC installation. RO treatment is furthermore known for its excellent desalinization properties. Over 90% monovalent ion rejection is possible with RO membranes, and low or no selectivity for monovalent ions is observed (Malaisamy et al., 2011). However, RO treatment suffers from low permeate flux, high

operating pressure and high energy requirements. It produces a difficult to treat saline concentrate, and sometimes remineralization of the permeate is required to make the water potable (Ilyas et al., 2017; Te Brinke et al., 2020a). Moreover, an extensive pretreatment is necessary. This together with the high energy consumption makes RO a costly treatment technique.

2.2.3 Direct NF of surface water with hollow fiber LbL membranes

An ideal membrane for the treatment of VM water would exhibit the flux behavior of NF (resulting in a lower energy consumption) and rejection behavior of RO membranes towards (monovalent) salts and small OMPs. A disadvantage of most commercially available NF and RO membranes is that they are flat sheet membranes in a spiral wound module, which have limited hydraulic and chemical cleaning possibilities, while hollow fiber membranes are much more resistant to fouling and have a higher surface area (De Grooth et al., 2014; Reurink et al., 2018). Their higher permeability also reduces energy consumption (Van der Bruggen et al., 2003). However, due to this higher permeability, retentions can be lower.

Hollow fiber polyamide ultra- or nanofiltration membranes can be modified by coating them with different polyelectrolyte multilayers (PEMs) to improve many aspects of their performance. PEMs have for example been used to make membranes low fouling, bipolar, ion selective and solvent resistant (Malaisamy et al., 2011; De Grooth et al., 2015). PEMs are fabricated by alternatingly exposing the membrane to positively and negatively charged polyelectrolytes, forming thin layers on the membrane. Most membranes are terminated with polyanion, as this shows to have a higher OMP retention than membranes terminated with polycation (Te Brinke et al., 2020a), and they are less prone to fouling (Te Brinke et al., 2020b). Due to their fouling-resistance and ease of cleaning, with these modified membranes the requirement of an extensive pre- and sometimes also post-treatment is eliminated (Van der Bruggen et al., 2003). Feed water can be applied almost directly, sometimes only preceded by a micro strainer, being a major advantage.

A polyelectrolyte pair that has been applied is the polycation poly(allylamine hydrochloride) (PAH) and polyanion poly(acrylic acid) (PAA), but these membranes have a very low permeability and are thus very energy-consuming (Te Brinke et al., 2020a). Abtahi et al. (2018) investigated the removal of different pharmaceuticals from treated municipal wastewater with PAH/PAA coated membranes and reached 44-77% rejection with NaCl retention around 17%. Ilyas et al. (2017) achieved 60-80% retention of both charged and neutral OMPs of varying size from 200-400 $gmol^{-1}$. These retentions were achieved at a low water permeability of 1.8 $Lm^{-2}\,h^{-1}\,bar^{-1}$ (Ilyas et al., 2017). Additionally, the PAH/PAA membranes show low chemical stability (De Grooth et al., 2015).

Multilayers based on PAH and polyanion poly(sodium 4-styrenesulfonate) (PSS), terminated with PSS, form very stable membranes with a high permeability (13-16 $Lm^{-2}\,h^{-1}\,bar^{-1}$) (Te Brinke et al., 2020a). This membrane type shows high salt retentions but smaller OMPs unfortunately still show significant permeation (Reurink et al., 2019). Te Brinke et al. (2020a) combined PAH/PSS (high permeability) and

PAH/PAA (high selectivity) coatings and achieved a very high retention of 98% toward a mix of common OMPs (in the range of 216-624 Da), while retaining 10-15% of NaCl at a permeability of 12.8 Lm^{-2} h^{-1} bar^{-1}. A PAH/PSS coating with a single final layer of Nafion, a polymer commonly used in the production of ion exchange membranes, increased the density of the membrane, resulting in a low MWCO of 287 Da. A cocktail of 8 small OMPs was removed up to 97% by these PSS/PAH/Nafion membranes (Reurink et al., 2019). Furthermore, retention towards NaCl, $MgCl_2$ and $MgSO_4$ were 55, 98 and 98%, respectively.

A commonly applied polyelectrolyte pair is the polycation poly(diallyldimethylammonium chloride) (PDADMAC) and PSS due to its excellent separation properties and high stability (Reurink et al., 2018). De Grooth et al. (2015) showed that this PDADMAC/PSS based membrane was very stable towards sodium hypochlorite (NaOCl). When the polyzwitterion poly N-(3-sulfopropyl)-N-(methacryloxyethyl)-N,N-dimethylammonium betaine (PSBMA), which carries both a positive and a negative charge, was incorporated into the PDADMAC/PSS layer, salt rejections of up to 42% NaCl, 72% $CaCl_2$, and 98% Na_2SO_4 were reached with permeabilities of 3.7-4.5 Lm^{-2} h^{-1} bar^{-1} (De Grooth et al., 2014). In addition, excellent removal of 6 diverse OMPs with molecular weights between 215 and 362 $gmol^{-1}$ was reached. Menne et al. (2016) coated ceramic support membranes with polyelectrolyte films, assembled from PDADMAC and PSS. The ceramic support is more expensive than a polyamide membrane but it can be reused as the PEMs are regenerable. The MWCO was determined to be 240 Da and the $MgSO_4$ retention 80-90%. However, this type of membrane has not been established in the market yet.

Most (PEM coated) hollow fiber polyamide NF membranes still need further optimization and are – to the writer's best knowledge – not yet commercially available. Pentair X-Flow (Enschede, The Netherlands) produces a polymeric NF hollow fiber membrane (HFW1000) with a MWCO of 1000 Da, but this was not designed to remove OMPs of small size (Ilyas et al., 2017). In addition, this chlorine tolerant membrane has limited reduction of bivalent salts, let alone of monovalent salts. NX Filtration (Enschede, The Netherlands) developed a capillary NF membrane suitable for the direct treatment of surface water, with the capacity of removing medicine residues, microplastics and endocrine disruptors from water – according to the manufacturer. The PEM coated dNF40 membrane with an estimated MWCO of 400 Da seems to be the most promising option for the filtration of VM water as it can also remove (monovalent) salts. Furthermore, it can operate at a water permeability of ~7 Lm^{-2} h^{-1} bar^{-1}, making the 1-step process energy efficient. Other advantages are the chlorine resistance of the backwashable membrane and its low fouling potential.

2.3 Configuration and structure of polyelectrolyte NF membranes

Hollow fiber NF is a pressure-driven membrane technology (Wang et al., 2011), operating at low pressures of about 3-5 bar. In general, there are two process modes for membrane filtration: dead-end and cross flow modes (Wang et al., 2011), which are both depicted in Figure 1. In case dead-end is applied, the entire feed flow is transported perpendicularly, depositing the substances to be separated on the membrane. Hollow fiber membranes however operate in cross-flow mode, where the feed flows parallel to the membrane surface, thereby being split into two streams. The stream that passes the semi-permeable membrane under the driving pressure is the permeate; the remaining stream on the feed side the concentrate (Wang et al., 2011).

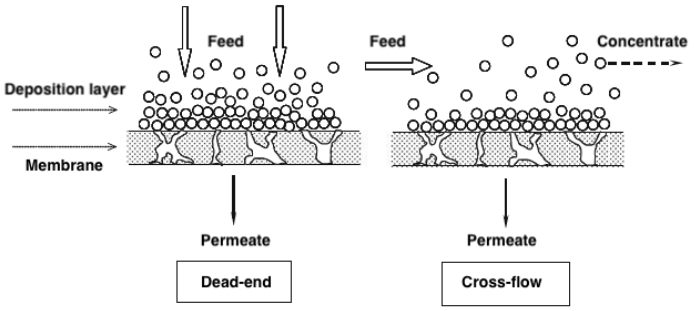

Figure 1. Dead-end and cross-flow filtration modes. Adapted from Wang et al. (2011)

In a full-scale hollow fiber NF membrane unit, about 13,000 long, fibers – or 'straws', often made of the polymeric material polyethersulfone (PES) – with very small diameter of 0.7 mm are packed together in a PVC casing as presented in Figure 2. The voids between the fibers are potted at the ends with an epoxy resin (Wang et al., 2011) to be able to separate the permeate water that has collected between the fibers from the concentrate water. For the treatment of surface water, inside-out filtration is mostly applied, having the smallest pores at the inside of the fiber (De Grooth et al., 2015). The active layer is thus located on the inside of the membrane.

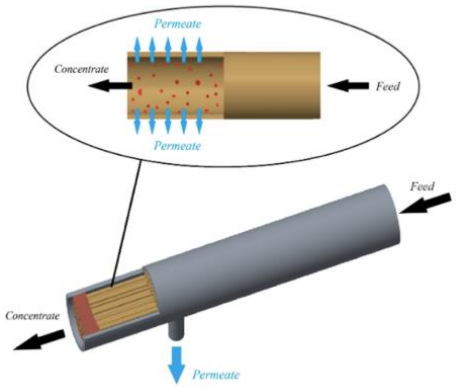

Figure 2. Schematic of feed flow through a hollow fiber NF membrane unit. Source: https://filtsol.com/main/index.php/technical-info/hollow-fiber-membranes.

Commercial polymeric NF membranes consist of thin-film composite (TFC) membranes, which are mostly negatively charged due to the dissociation of functional groups – mostly carboxylic acid groups – on the surface membrane (Verliefde et al., 2007b; Cheng et al., 2018). The negatively charged surface promotes the repulsion of anions over cations as negatively charged compounds cannot approach the negatively charged membrane due to electrostatic repulsive forces. PEMs are promising materials to overcome the problems of demineralization and highly saline concentrates that occur with traditional NF as they only partly remove salts (Te Brinke et al., 2020a). PEMs can be coated on surfaces, including porous membrane supports, by applying the LbL technique (Reurink et al., 2018), which was introduced by Decher et al. in the early nineties (De Grooth et al., 2015). The membrane is alternatingly exposed to positively and negatively charged polyelectrolytes, forming thin layers on the membrane as shown in Figure 3. The surface charge of the membrane is determined by the charge of the terminal layer.

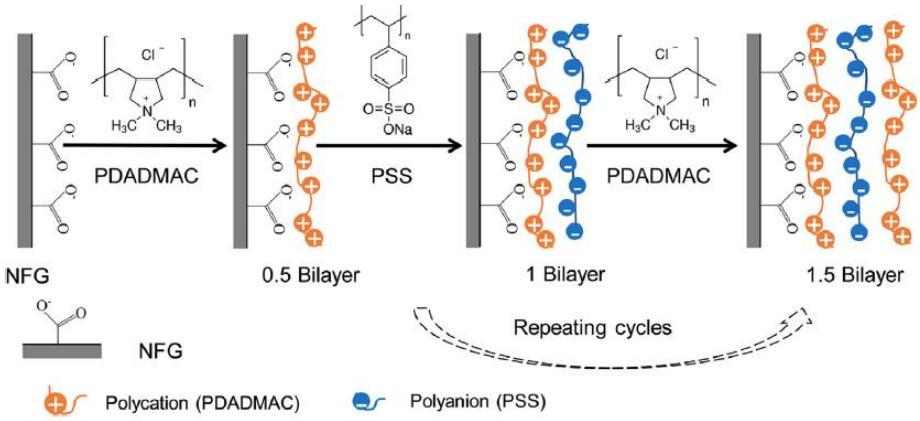

Figure 3. Fabrication of polyelectrolyte multilayers (PEMs) with alternating deposition of polycation (PDADMAC) and polyanion (PSS) on the polyamide NF membrane (NFG). Source: Cheng et al. (2018)

Membranes terminated with a negatively charged PDADMAC layer have a higher rejection of divalent cations and selectivity for Na^+ transport over divalent cations, thereby removing a part of scale-forming cations (Cheng et al., 2018). However, to prevent scaling and (bio)fouling, the membranes need to be cleaned regularly. This can be done physically – by means of backwashing or forward flushing – or chemically – e.g., by pH changes or oxidation to remove strongly bound fouling (De Grooth et al., 2015). De Grooth et al. (2015) investigated the chemical degradation of PEM modified membranes in the presence of sodium hypochlorite. The type of polycation proved to be an important factor in the chemical stability: membranes coated with PDADMAC were stable for more than 100,000 ppm hours NaOCl at pH 8 (De Grooth et al., 2015).

An unfortunate phenomenon that can occur during multilayer coating is overcompensation by PDADMAC. Reurink et al. (2018) showed that this overcompensation results in a positively charged surface even though the multilayer is terminated with PSS, which leads to poorer retention efficiencies (for instance a decrease of SO_4^{2-} retention from 94 to 39%). Fortunately, recovery of the negative surface can be obtained by a so-called annealing cycle with a high salt concentration.

2.4 Transport mechanism – the Nernst Planck Model

A membrane is a barrier between two phases. A molecule or particle crosses this boundary due to a driving force such as a pressure difference acting on that molecule or particle (Wang et al., 2011). The PEM-coated hollow fiber NF membranes are *dense* membranes to which the non-porous solution-diffusion model applies, where solutes dissolve at the membrane interface and then diffuse through the membrane along the concentration gradient (Wang et al., 2014). In the extended Nernst Planck equation, which is stated in Equation (1), solute transport is described as a combination of diffusion, convection and electro-migration. The flux, J_i, of a solute i with charge z_i through a membrane pore is

$$J_i = J_w C_{i,p} = -K_{i,d} D_i^{\infty} \frac{dc_i}{dx} + K_{i,c} c_i J_w - \frac{z_i c_i K_{i,d} D_i^{\infty} F}{R_g T} \frac{d\psi}{dx} \quad (1)$$

where D_i^{∞} is the solute diffusion coefficient at infinite dilution, $K_{i,d}$ and $K_{i,c}$ the diffusive and convective hindrance parameters, respectively, F is the Faraday constant, T the temperature, R_g the universal gas constant and ψ the electrical potential within the pore length (Wang et al., 2014). Water and solutes are transported towards the membrane surface by convection. Water permeates, and solutes can either pass the membrane or be repulsed and transported back to the feed bulk. The first term represents diffusive and the second term indicates convective (pore-flow) transport through the membrane. The final term describes the electro-migration.

2.5 Retention mechanisms

In NF, steric (size) and Donnan (charge) exclusion are the main rejection mechanisms (Cheng et al., 2018). Both mechanisms are discussed in this section, as well as the phenomenon of solute-membrane affinity.

2.5.1 Steric rejection: the 'sieve effect'

Size exclusion is the main removal mechanism for neutral OMPs: the larger the molecule, the lower its passage (Albergamo et al., 2019). Rejection of uncharged particles in NF often increases with increasing particle molar mass. When the molar mass of an uncharged compound is higher than the MWCO of the membrane, retention of that compound is usually high (Verliefde et al., 2007a). The rejection is a result of the sieving effect of the membrane polymer network as the molecular size of the particle is larger than the pore size (Verliefde et al., 2007a). Charged molecules can also be separated based on their size. Considering ions, multivalent ions are retained more favorably than monovalent ions by NF membranes, due to their larger hydrated size and charge (Cheng et al., 2018). Both Na^+ and Cl^- have a small diameter of 0.2 nm (Marcus, 1988), which makes it particularly difficult to remove them. They are much smaller than OMPs that typically have a diameter of about 1 nm (Te Brinke et al., 2020a).

2.5.2 Donnan exclusion: the repulsion effect

High rejection of negatively charged organic solutes by NF membranes has been reported as a result of electrostatic interactions between the membrane and the solute (Bellona & Drewes, 2005; Verliefde et al., 2007b). Furthermore, salt rejection is mainly caused by electrostatic interactions between ions and the NF membrane (Wang et al., 2011). Most commercial thin-film composite NF membranes are negatively charged at neutral pH due to the dissociation of acidic functional groups on the membrane surface and have a repulsing effect on negatively charged compounds (Verliefde et al., 2008; Cheng et al., 2018). The surface charge of PEM NF membranes are determined by the top layer of the coating (Cheng et al., 2018). As most PEM membranes are terminated with polyanion, they are also negatively charged.

Electrostatic forces prevent attachment of anions as they cannot approach the membrane. Next to this repulsion of co-ions, the membrane attracts counterions and as a result a so-called Donnan equilibrium arises at the membrane interface (as represented in Figure 4).

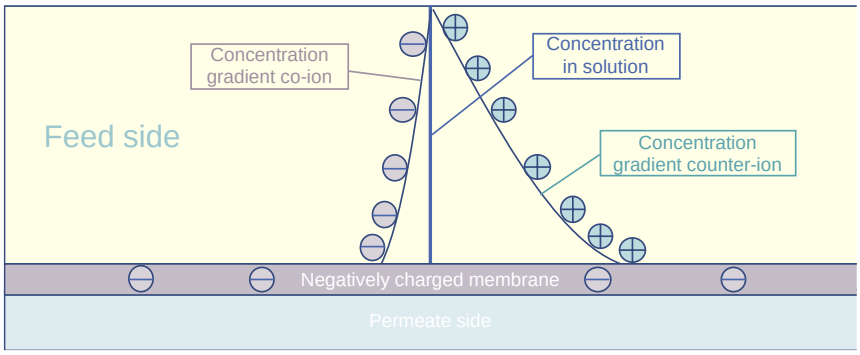

Figure 4. Representation of the Donnan equilibrium, where the concentration of co-ions is lower at the membrane surface than in the solution, while the concentration of counter-ions is higher.

A positively charged 'shield' is formed at the membrane surface which is the inner region (the Stern layer) of the electric double layer. In the outer, diffuse layer, ions move around freely. The maximum potential appears at the negatively charged surface and decreases across the Stern layer due to the presence of positively charged ions, resulting in what is defined as the zeta potential (Moussa et al., 2017). The potential difference prevents the passage of anions to the permeate side. The requirement for electroneutrality in the feed water (2) leads to a retention of cations as well (Ong et al., 2002). Meanwhile, electroneutrality also applies to the permeate water (3): when cations pass the membrane, they need to carry an equal charge of anions to the permeate side.

$$\sum_i z_i c_{i,feed} = 0 \qquad (2)$$

$$\sum_i z_i c_{i,permeate} = 0 \qquad (3)$$

2.5.3 Solute-membrane affinity

Hydrophobic OMPs are also influenced by solute-membrane affinity interactions (Verliefde et al., 2009c; Albergamo et al., 2019). Due to affinity between hydrophobic sites – such as aromatic rings and hydrocarbon chains – and the charged layer of the membrane, these OMPs can adsorb onto the membrane. Commercial membranes are often composed of relatively hydrophobic polymers and affinity between hydrophobic solutes and hydrophobic polymers is high (Verliefde et al., 2009c). Consequently, a high rejection will initially be observed, but once membrane saturation is reached, the adsorbed OMPs can move through the membrane and diffuse to the permeate side (Albergamo et al., 2019). This effect results in a lower retention.

2.6 Operational parameters

2.6.1 pH and temperature

pH does not only influence the charge of a solute, but also the charge of a membrane (Verliefde et al., 2007a), thereby affecting retention values. Several studies of flat-sheet NF membranes demonstrated that the rejection of negatively charged compounds increased with increasing feed pH due to a more negative surface charge of the membrane, which increased electrostatic repulsion (Bellona & Drewes, 2005; Verliefde et al., 2009c). In addition, recently was shown that an increase in temperature could lead to an increase in pore size of NF membranes as well as an increase in permeate flux, resulting in lower retentions of OMPs (Xu et al., 2020). In this study, constant pH and temperature were applied to obtain comparable results.

2.6.2 Feed composition

In membrane filtration, feed composition and concentration have an effect on the retention of ions and OMPs. It is well-known that divalent ions are often better retained than monovalent ions, but amongst monovalent anions, selectivity also plays a role: the presence of fluoride in a water matrix for example influences Cl^- rejection (Malaisamy et al., 2011). The concentration of the feed also has an effect on salt transport; Ong et al. (2002) reported a decrease in salt retention with increasing feed salt concentration. Furthermore, the ionic composition showed to affect the rejection of target micropollutants with flat-sheet NF membranes (Sanches et al., 2012). For the PEM NF membranes, the applied water should not be too salty. Saline feed water diminishes the charge effect of the surface and leads to swelling of the multilayers. Therefore, it is recommended to only treat waters with mild-salinity (Cheng et al., 2018).

2.6.3 Cross-flow velocity

The crossflow velocity is the tangential flow through the membrane from feed side to concentrate side (Wang et al., 2011). The velocity in the fibers should be sufficiently high to prevent concentration polarization, which can lead to fouling or scaling. This phenomenon is further discussed section 2.7.

2.6.4 Permeate flux

The performance of a membrane can be expressed in terms of the permeate, or water flux, which is defined as the amount of permeate produced per unit area of membrane surface per unit time (Wang et al., 2011). The 'productivity' of the membrane can be described by:

$$J_w = \frac{K_w}{\mu} \cdot (\Delta P - \Delta \pi) \quad (4)$$

where J_w is the water flux, μ is the dynamic viscosity, K_w the water permeability of the membrane, ΔP the transmembrane pressure (TMP) – the average applied hydraulic pressure over the membrane – and $\Delta \pi$ the osmotic pressure difference across the membrane. The water flux increases linearly with increasing applied pressure. Moreover, salt rejection increases with both water flux and applied pressure (Wang et al., 2014), as increasing the operational pressure results into a larger flow of water through the membrane. While the increase in water flux is larger than the increase of the solute flux, retention will hence increase.

2.6.2 Hydraulic pressure loss

When water flows through the membrane fibers, the friction between the feed water and the fiber walls causes pressure loss (Wang et al., 2011). The flow in the fibers is expected to be laminar. The hydraulic pressure loss ΔP_H, or the pressure drop over the length of the membrane, can hence be described by Darcy-Weisbach's model for cylindrical pipe flow, as stated here:

$$\Delta P_H = \lambda \cdot l \cdot \frac{\rho}{2} \cdot \frac{{v_{cf}}^2}{d_i} \quad (5)$$

where λ is the friction factor that for laminar flow which can be described by $\lambda = \frac{64}{Re}$ and $Re = \frac{d_i v_{cf} \rho}{\mu}$, l is the length of the fiber from feed to concentrate side, ρ is the density of the fluid, v_{cf} the cross-flow velocity and d_i the inner diameter of a fiber. Hydraulic resistance can increase due to fouling behavior (Zularisam et al., 2006).

2.6.3 (System) recovery

Recovery (γ in %) is an important parameter in filtration processes as it expresses the ratio of the volume of permeate produced (V_p in m^3) to the volume of feed water (V_f in m^3):

$$\gamma = \frac{V_p}{V_f} \cdot 100\% \quad (6)$$

The once-through recovery of a single full-scale NF element is approximately 7-10%. Higher recoveries can be reached by connecting multiple elements in series – where the concentrate of the first element continues as feed water for the next element, and so on – or by a co-called feed-and-bleed configuration. In this latter arrangement, a part of the concentrate is recirculated over the membrane. Multiple stages can be introduced to increase the overall system recovery. The feed water thus becomes more and more concentrated towards the final stage, thereby adversely affecting the retention of ions and solutes. Although this leads to deterioration of the average permeate quality, high system recoveries are often desired to restrict concentrate volumes. On the contrary, a high system recovery results in a concentrated waste stream (Verliefde et al., 2009b) of which disposal can become an issue. Nederlof et al. (2005) emphasized the necessity of discussing disposal options with the water authority before engineering the installation. Parameters such as SO_4^{2-}, Cl^-, PO_4^{3-} and Fe^{2+} are often an issue.

2.7 Fouling mechanisms

2.7.1 (Bio)fouling

Membrane fouling is considered as the main obstacle in membrane filtration efficiency, especially in high pressure NF or RO spiral wound elements, as it causes flux decrease and permeate quality decline (Zularisam et al., 2006; Verliefde et al., 2009a; Botton et al., 2012). Membrane fouling can refer to: (i) *biofouling*, which is microbial in origin; (ii) *organic fouling* due to the accumulation of NOM on the surface of the membrane; (iii) *colloidal fouling* as a consequence of the accumulation of small colloidal particles in the feed water on the membrane surface; or (iv) *scaling*, which is discussed separately in the following section (Verliefde et al., 2009a). Deposition of retained solutes on the membrane surface is generally referred to as a ‘gel cake layer’ (Zularisam et al., 2006). However, solutes can also cause pore blockage or adsorb onto the membrane surface, which increases the hydraulic resistance and thereby decreases the flux (Wang et al., 2011).

For flat-sheet NF membranes it was found that deposition and growth of biofilm on the membrane surface can slightly increase the surface charge, becoming more negative (Botton et al., 2012). The negatively charged biofilm enables positively charged OMPs to accumulate in the biofilm, which reduces their rejection as diffusion back to the bulk solution is hindered (Botton et al., 2012). Untreated surface water contains colloidal particles as well as NOM molecules (Verliefde et al., 2009a). An extensive pretreatment is required to remove foulant material when membrane filtration is applied to this water type. PEM coated hollow fiber NF membranes on the other hand showed to be quite resistant to fouling (Arun, 2019), which can be dedicated to the lack of spacers and larger fouling interface, while they can be cleaned very well physically (Ilyas et al., 2017). However, NOM can still interfere with retentions as the negatively charged organic material can bond with the polycation layers in the membrane, thereby neutralizing the charge of these layers.

2.7.2 Scaling

During membrane filtration, localized concentration of salt builds up at the boundary layer of the membrane, which is called ‘concentration polarization’ (CP) (Wang et al., 2011). Solutes can also contribute to this phenomenon. For positively charged solutes, charge interactions with the negatively charged membrane surface exist, which causes an increased concentration of positively charged particles at the membrane surface compared to the concentration in the feed water (Verliefde et al., 2008). High CP reduces the water flux and increases the salt flux through the membrane, thus increasing the salt concentration in the permeate (Wang et al., 2011). When the concentration close to the membrane exceeds the solubility product, inorganic deposition occurs on the membrane surface, which is also referred to as *scaling* (Verliefde et al., 2009a). Concentration polarization can be reduced by increasing cross-flow velocity and creating turbulence (Wang et al., 2011).

3

Materials and methods

3.1 Experimental set-up

In Figure 5, a piping and instrumentation diagram (P&ID) of the MexPlorer basic test unit, designed by NX Filtration (Enschede, The Netherlands), is shown. The details are provided in Table 1. The temperature of the feed water was controlled by a cooling bath in which the feed tank (1) was placed. The feed water was pumped through the system by a high-pressure pump (2). A pressure relief valve (3) prevented equipment failure as a result of pressure build up. A strainer of 100 micron (4) was put prior to the NF module to sieve out particles that could potentially block the fibers. Flow through the pipes could be controlled by opening or closing the gate valves (5). The pressure of the feed and concentrate was regulated by partially closing the valve on the concentrate side, while the feed and permeate valve remained fully opened. Pressure indicators displayed the pressure of the feed, concentrate and permeate stream (PIF, PIC, PIP). The feed flow was controlled by adjusting the speed of the variable frequency drive pump, operating in cross-flow mode. A rotameter (6) was connected to read the flow.

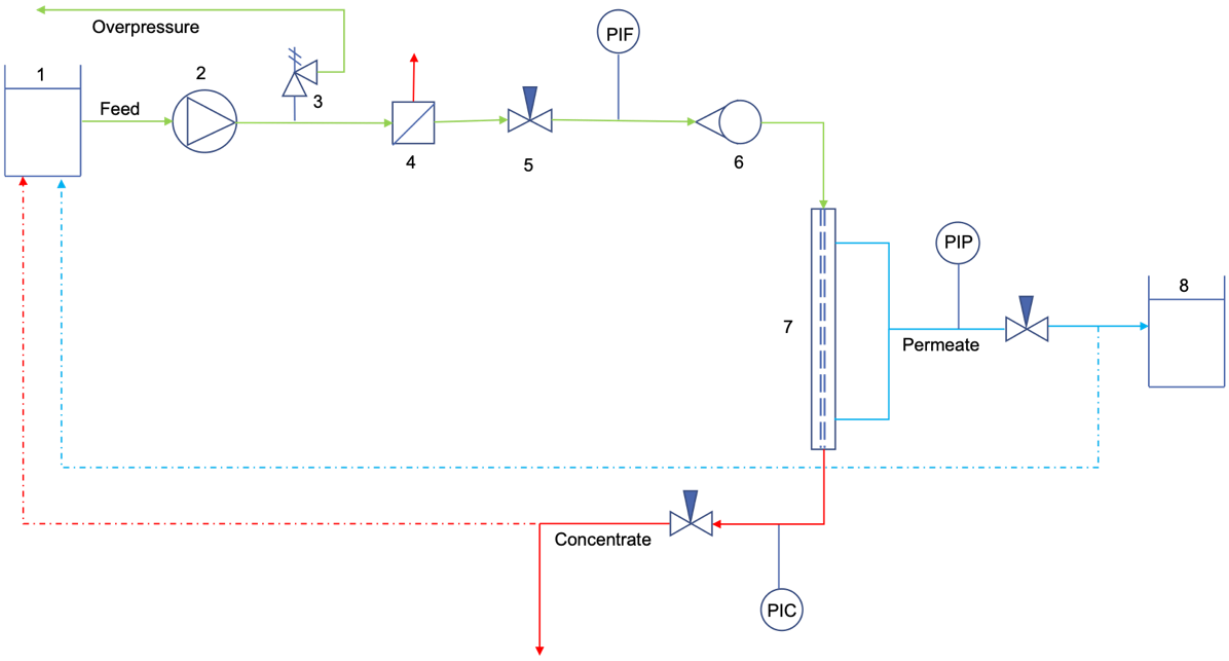

Figure 5. P&ID MexPlorer lab scale installation NX Filtration

The cross-flow velocity could be calculated from the feed flow by:

$$v_{cf} = \frac{q_{feed}}{n \cdot A_{cross-section}} \quad (7)$$

where q_{feed} is the feed flow in m^3s^{-1}, n (-) the amount of fibers in the module and $A_{cross-section}$ the cross-sectional area of a single fiber in m^2, given by $A_{cross-section} = \frac{\pi}{4} * d_{inner}^2$. No flow meter was provided for the permeate flow, so this was measured by hand with a graduated cylinder. Subsequently, the permeate flux J could be determined by the general equation for membrane processes (Wang et al., 2011):

$$J = \frac{q_{permeate}}{A_{filtration}} = \frac{q_{permeate}}{n \cdot l \cdot \pi \cdot d_{inner}} \quad (8)$$

where J is in $Lm^{-2}h^{-1}$, $A_{filtration}$ the active filtration area in m^2, n (-) the amount of fibers in the module, l the effective length and d_{inner} the average inner diameter of the fibers (both in m). All connection pipes were made of PVC (PN10 and PN16 by John Guest).

Table 1. Legend P&ID MexPlorer (Figure 4)

Label	Name	Information
1	Feed tank	10 or 20 L
2	Rotary vane pump	model PO211 by Fluid-o-Tech
3	Pressure relief valve	-
4	Microfilter	100 micron by Amiad
5	Gate valve	-
6	Rotameter	25-250 Lh^{-1}
7	Membrane element	dNF40 by NX Filtration
8	Permeate tank	10 or 20 L
PIF	Pressure indicator feed	0-10 bar by WIKA
PIP	Pressure indicator permeate	0-10 bar by WIKA
PIC	Pressure indicator concentrate	0-10 bar by WIKA

When the feed water entered the fibers of the membrane (7) – inside-out configuration –, this stream was split into a permeate and a concentrate stream. Dependent on the experiment, the permeate and concentrate streams were collected separately or recycled back to the feed tank. The dNF40 membrane element was also supplied by NX Filtration. The specifications of the membrane module are shown in Table 2. The modified PES dNF40 membranes with a negatively charged terminal layer have an estimated molecular weight cut-off (MWCO) of 400 Da and a hydraulic permeability of pristine membranes of 7 $Lm^{-2}h^{-1}bar^{-1}$ at 25 °C according to the supplier. The filtration area was calculated to be 0.079 m^2.

Table 2. Specifications of the dNF40 lab scale membrane module, provided by the supplier

Parameter	Value	Unit
Diameter fiber	0.7	mm
Number of fibers	120	-
Length fiber	300	mm
Membrane material	Modified PES	-
Charge membrane	Negative at pH 7	-
Operation	Inside-out, cross-flow	-
Est. bacteria rejection	>6 log	-
Est. virus rejection	>5 log	-
Max. TMP	6	bar
Max. operating temperature	50	°C
Operating pH range	1-14	-

3.2 Filtration experiments

Filtration experiments were carried out with different water types. The single pass water recovery of the hollow fiber NF module was 1-2%. In addition, the permeate and the concentrate were fed back to the feed tank – except for the sampling volume, which was a negligible amount (<2.3%). This way the composition of the feed water remained fairly constant over the duration of the experiment. The samples were taken during filtration to monitor the retention of the ions or molecules of interest. The retention R_i in % was calculated using the equation below.

$$R_i = \left(1 - \frac{c_{i,p}}{c_{i,f}}\right) \cdot 100\% \quad (9)$$

where $c_{i,p}$ is the concentration in the permeate and $c_{i,f}$ the concentration in the feed water. The experiments were performed at room temperature with a transmembrane pressure of 2.0-5.0 bar, and a flux of 10-27 $Lm^{-2}h^{-1}$, which is a common flux for this type of membrane (Jährig et al., 2018). The applied cross-flow velocity was 0.4-1.0 ms^{-1}, resulting in a Reynolds number (Re) of 790 or lower, which indicates laminar flow in the fibers. The experimental conditions are summed up in Table 3.

Table 3. Experimental conditions

Parameter	Value(s)	Unit
Cross-flow velocity	0.4, 0.6, 0.7, 1.0	ms^{-1}
Permeate flux	10, 18, 27-28	$Lm^{-2}h^{-1}$
TMP	2.0, 3.5, 5.0	bar
Nominal pressure drop	0.2	bar
Temperature	21	°C

3.2.1 Hydraulic permeability

Before the filtration experiments, a filtration test with demineralized water was performed to determine the initial hydraulic permeability. The following equation was used to calculate the temperature-corrected permeability, in case the temperature of the feed water had increased slightly:

$$L_{21°C} = \frac{J \cdot e^{-0.0239(T-20)}}{\Delta P} \quad (10)$$

where $L_{20°C}$ is the temperature-corrected permeability at 20°C in $Lm^{-2}h^{-1}bar^{-1}$, T the temperature of the water in °C, J the permeate flux in $Lm^{-2}h^{-1}$, and ΔP the transmembrane pressure in bar, which is defined as:

$$\Delta P = P_{feed} - \frac{\Delta P_{hydraulic}}{2} - P_{permeate} \quad (11)$$

where P_i is the pressure of the feed, or permeate in bar and $\Delta P_{hydraulic}$ the hydraulic pressure loss along the fiber. For pure water and low salt concentrations, the osmotic pressure difference between the feed and permeate is equal to zero. To determine the hydraulic permeability, the permeate flux was measured at TMPs of 2.0, 3.0, 3.5, 4.0 and 5.0 bar.

3.2.2 Molecular weight cut-off

A mixture of five polyethylene glycol (PEG) polymers with different molecular weights of 200, 300, 400, 600 and 1000 Da (Sigma-Aldrich), each in a solution of 0.6 gL^{-1} with demi water, was filtrated. Control tests with single solutions of 200 and 300 Da were also performed, as larger molecules in the mixture potentially can block the pores, leading to an overestimation of the MWCO (Shang et al., 2017). The PEG molecules are non-charged, so their retention is the result of steric rejection. Samples were collected as presented in Figure 6. Standard solutions of each PEG molecule were prepared in the same concentration. Then, the feed and permeate samples and the standards were filtered using a 0.45 μm filter before being analyzed by high-performance liquid chromatography (HPLC, Shimadzu) equipped with size exclusion chromatography columns. When passing through the columns, each molecule showed a different elution time, corresponding with its molecular weight (MW). From the height of the peak, the concentration of a specific molecule could be determined. From the HPLC analyses, molecular weight distribution curves could be derived, which were converted into retention curves. Subsequently, the experimental retention curves were described by a log-normal model as a function of MW and MWCO:

$$\sigma(MW_s) = \int_0^{MW_s} \frac{1}{S_{MW}\sqrt{2\pi}} \cdot \frac{1}{MW} \cdot exp\left[-\frac{(\ln(MW) - \ln(MWCO) + 0.56S_{MW})^2}{2s_{MW}^2}\right] dMW \quad (12)$$

Where $\sigma(MW_s)$ is the reflection coefficient for a PEG with a molecular weight MW_s and with S_{MW} as the standard deviation of the molecular weight distribution (Kramer et al., 2019).

A correlation between the molecular size of PEG molecules and their molecular weight, where the pore size of the NF membrane is assumed to follow a log-normal distribution and solute diffusion is expected negligible, can be described by the following equation (Shang et al., 2017):

$$d_s = 0.065 \cdot (MW)^{0.438} \qquad (13)$$

with d_s the diameter in nm and molecular weight MW in Da. Finally, the MWCO was estimated at 90% of the retention curve (Kramer et al., 2019).

3.2.3 Filtration with SW

To mimic the ionic composition of VM water, first two mother stock solution were prepared. In solution A, 4.90 gL^{-1} $CaCl_2$ (Honeywell) and 2.24 gL^{-1} $MgCl_2$ (Sigma) were dissolved in 1 L tap water. In solution B, 2.27 gL^{-1} Na_2SO_4 (Carl Roth) and 6.15 gL^{-1} $NaHCO_3$ (J.T. Baker) were dissolved, also in 1 L tap water. The tap water was provided by Dunea from production location Scheveningen. To reach the desired ionic composition, 0.3 L from each stock solution was taken and filled up to 20 L with tap water in a tank. pH adjustment was not necessary as the pH was already in the same range. No model compounds were used for microbes, algae, or other NOM which are present in surface water. The exact composition of tap water from Dunea and the SW can be found in Table 4 in section 3.4.1. To investigate the effect of different Cl concentrations, the Cl concentration was increased by adding NaCl (Boom) to the SW. To reach 200 mgL^{-1} Cl, 2.25 mgL^{-1} NaCl was added to 20 L and 5.84 mgL^{-1} NaCl was added to 20 L obtain 400 mgL^{-1} Cl. Filtration with SW was performed to determine the effect of feed concentration, permeate flux, cross-flow velocity, and system recovery on rejection.

In the experiments with OMPs, the SW was spiked with a mixture of 20 OMPs which are listed in section 3.4.2. From this mother stock solution, 1 mL was added per 10 L of water to obtain concentrations in the range from 0.2-10 μgL^{-1}. To avoid possible degradation, the stock solution was stored in an amber glass bottle and kept in the freezer (−18°C). The solutions with OMPs were prepared immediately before starting the filtration experiment. Adsorption of OMPs onto the charged membranes can lead to higher apparent retention. To avoid overestimation of OMP rejection, several authors recommended a stabilization period of 24h (Kimura et al., 2003; De Grooth et al., 2014; Ilyas et al., 2017; Reurink et al., 2019) and some even of 48h or longer (Verliefde et al., 2008; Abtahi et al., 2018). To investigate if membrane saturation was already reached within 24h, experiments with spiked SW were conducted after both 24h and 48h of stabilization. During stabilization, the permeate and concentrate were circulated back to the feed tank.

3.2.4 Filtration with VM water

VM water, with a total volume of 70 L, was collected on 9 September 2020 at ~0.5 m below the water surface using a hand pump. In contrast to the SW, VM water contained nutrients such as PO_4^{3-}, and organic material such as algae and micro-organisms. The composition is also shown in Table 4 in section 3.4.1. Salt retention was investigated at different permeate fluxes and system recovery values. The retention of OMPs was researched by spiking the VM water in the same way as described above in the experiments with SW. From the comparison with SW after 24h and 48h of stabilization could be concluded that saturation of the membrane was accomplished within 24h. Therefore, stabilization of spiked VM water was carried-out for 24h.

3.2.5 Cleaning the membranes

After all experiments with SW (without OMPs), forward flush with demineralized water was conducted at 1.5 times the filtration velocity for 20 minutes. This measure was taken to remove possible build-ups of salts or NOM from the membrane surface. If scaling by ions was suspected, the membranes were cleaned with a citric acid solution with pH 2-4, and properly flushed afterwards. The 100-micron strainer was regularly cleaned by detaching it from the module and flushing out the accumulated particles. After each experiment with OMPs and/or VM water, the membranes were chemically cleaned with a high pH solution followed by a low pH solution. First, a solution of 200 ppm NaOCl at a pH of 10-12 (with NaOH) was circulated through the system for 20 minutes at low pressure without producing permeate. The membranes were subsequently soaked for 30 minutes, after which the module was flushed with water for 30 minutes to remove all hypochlorite. Second, a citric acid solution with pH 2-4 was used to avoid scaling. After this cleaning cycle, the module was again properly flushed. When the system was not operating, the membranes were submerged in demineralized water to prevent the fibers from drying out.

3.3 Sampling

At the start of each experiment, demineralized water was recirculated through the system for 20 minutes, after which gravity drainage was applied to remove all water from the system. In total, 5 samples of 15 mL each were taken per experiment: 2 of the feed and 3 of the permeate. The first samples of the feed (F1) and permeate (P1) were taken after 60 minutes of filtration. Permeate samples were collected every 30 minutes and feed samples every hour. Each experiment had a duration of 2 hours. An overview of the taken samples is shown in Figure 6.

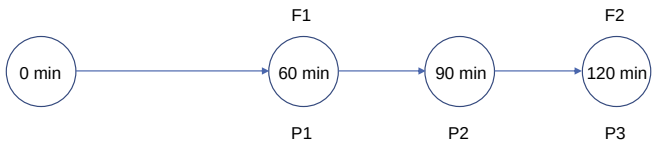

Figure 6. Sampling schedule of feed (F1-2) and permeate (P1-3) during each experiment with recycling

Before the start of the experiments with OMPs, the spiked SW was first recirculated for 24 hours to saturate the membranes. Afterwards, sampling took place in the same aforementioned way. Subsequently, recirculation was extended for another 24 hours to determine if membrane saturation had been reached after 1 day. The spiked VM water was also recirculated for 24 hours before the start of the experiment.

Sampling during recovery experiments occurred in a slightly different manner, as depicted in Figure 7 below. During these experiments, the permeate was collected in a separate tank, while the concentrate was recycled back to the 10 L feed tank. A sample of the feed was taken at the beginning of the experiment (F0). Once the desired recovery of 25, 50 or 75% was reached, samples were taken of the feed (F1-3), the permeate produced at that specific system recovery (P1-3) and the collected mixed permeate (P_{mix}1-3) to determine the concentration factor of the feed water, the specific retention, and the average retention, respectively. These experiments were conducted twice in order to collect duplicates, leading to 20 samples in total per recovery experiment.

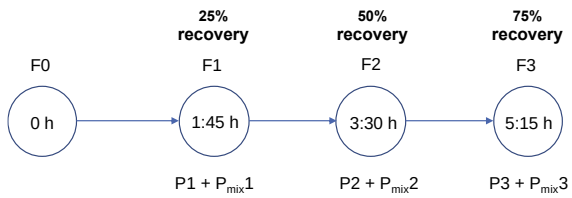

Figure 7. Sampling schedule of feed (F1-4), permeate (P1-3) and mixed permeate (P_{mix}1-3) during recovery experiments.

3.4 Composition of the water

3.4.1 Water matrices of Dunea tap water, SW and VM water

Table 4. Water composition of Dunea tap water (data from 18 August 2020), SW (with 3 different NaCl concentrations) and VM water. Some ions could not be detected (<d.l.) as their concentrations were very low.

Parameter	DW	SW	VM water	unit
pH	8.44	8.45	8.23	-
EC	547	875	1238	μScm^{-1}
		1093		
		1744		
turbidity	<0.03	<0.03	26.4	NTU
hardness	1.43	2.71	2.89	$mmolL^{-1}$
TOC	1.83	1.83	11.6	mgL^{-1}
NO_3^-	2.79	2.79	1.64	mgL^{-1}
NH_4^+	<0.02	<0.02	<d.l.	mgL^{-1}
PO_4^{3-}	0.13	0.13	<d.l.	mgL^{-1}
Na^+	51.3	89.7	153	mgL^{-1}
		130		
		255		
K^+	6.18	6.18	14.8	mgL^{-1}
Mg^{2+}	8.8	17.9	23.6	mgL^{-1}
Ca^{2+}	42.4	78.5	76.2	mgL^{-1}
F^-	0.22	0.22	<d.l.	mgL^{-1}
Cl^-	46.4	119	235	mgL^{-1}
		193		
		388		
Br^-	<d.l.	<d.l.	<d.l.	mgL^{-1}
HCO_3^-	172	240?	239	mgL^{-1}
SO_4^{2-}	46.7	67.4	90.3	mgL^{-1}
Ion balance	1.50	8.45	2.35	%

3.4.2 Selection of OMPs

When determining the rejection of OMPs by the dNF40 membrane, it is important to select OMPs which are representative for a typical range of physical-chemical properties of emerging contaminants such as pharmaceutical residues and endocrine disrupting compounds (Bellona & Drewes, 2005). In prioritizing OMPs, criteria such as human health risk, possible occurrence of high concentrations in drinking water sources, risk perception of the customer and low removal efficiency in treatment should be considered (Verliefde et al., 2007a).

In collaboration with Het Waterlaboratorium, 20 OMPs were selected. They are all pharmaceuticals that vary in size, charge and hydrophobicity. 20 L jerrycans were spiked with 2 mL of a concentrated spike solution to obtain the concentrations mentioned in the table below. The characteristics and chemical structures of the OMPs were obtained from PubChem.

Table 5. Physico-chemical characteristics of the selected OMPs.

Pharmaceutical	application	MW ($gmol^{-1}$)	pKa (-)	charge	Cfeed SW (μgL^{-1})	Cfeed VM (μgL^{-1})
amisulpride	antipsychotic	370	9.37	0	0.56	0.72
benzotriazole	industrial chemical	119	8.37	0	4.95	10.29
candesartan	antihypertensive	441	2.45	-	2.78	5.05
carbamazepine	antidepressant	236	15.96	0	4.32	4.91
citalopram	antidepressant	324	9.78	+	0.24	0.20
clarithromycin	antibiotic	748	8.99	+	1.67	1.82
diclofenac	anti-inflammatory	296	4.16	-	1.84	2.12
furosemide	antihypertensive	331	3.90	-	4.87	5.40
gabapentin	anti-epileptic	171	3.68	-	8.56	9.85
hydrochlorothiazide	antihypertensive	298	9.20	0	2.68	3.08
irbesartan	antidiabetic	429	4.08	-	2.48	5.11
metoprolol	antihypertensive	267	9.60	+	0.43	0.45
sotalol	antiarrhythmic	272	10.07	+	1.12	0.99
sulfamethoxazole	antibiotic	253	5.70	-	4.05	3.45
trimethoprim	antibiotic	290	7.12	+	0.85	0.91
venlafaxine	antidepressant	277	10.09	+	0.34	0.38
acetamidoantipyrine	pain killer	245	12.52	+	2.93	3.23
formylaminoantipyrine	pain killer	231	8.85	0	2.07	2.70
metformin	antidiabetic	129	12.4	+	3.47	5.98
valsartan	antihypertensive	436	4.73	-	2.04	2.37

3.5 Physical and chemical analysis

The feed flow was read from a rotameter connected to the Mexplorer. The permeate flux could be derived from the permeate flow, which determined using a graduated cylinder and stopwatch. The flux was monitored throughout the experiments. pH, temperature and electrical conductivity were measured using a calibrated Hach HQ40d portable multimeter. The 2100P ISO Turbidimeter was used for turbidity measurements. As described in section 3.2.2., high-performance liquid chromatography (HPLC, Shimadzu) analysis was used to determine the MWCO. The ions in the feed and permeate were analyzed by a ProfIC 15-AnCat ion chromatograph, Metrohm, 881 anion (suppressed) and 883 cation system, in the Waterlab of TU Delft. Prior to the analyses, the samples were filtered through 0.45 µm filters (Whatman). A Supp 5 150/4.0 anion column with 3.2 mM Na_2CO_3 and 1 mM $NaHCO_3$ eluent for anions was used. An A C6 150/4.0 cation column with 3 mM HNO_3 eluent was used for the cations. The suppressor was regenerated by a 150 mM H_3PO_4 solution.

HCO_3^- was analyzed by titration with 0.02 M hydrochloric acid with the Titrino, Metrohm, 848 plus. Total organic carbon (TOC) was determined by the TOC analyzer (Shimadzu). Inorganic carbon was first removed from the sample by acidifying and purging with oxygen. Subsequently, the sample water was oxidized at 720°C using a catalyst, after which the resulting CO_2 gas was measured. OMPs were measured using liquid chromatography-mass spectrometry with multi-stage mass-spectrometry (LC-MS-MSn). The OMPs were measured using a Water I-Class UPLC with a XEVO TQ-XS MS as detection system. An Acquity UPLC BEH C18 2.1x100 mm 1.7 µm column and a gradient method provided chromatographic separation of the OMPs. Due to the low concentrations of the components, there was both a basic and an acidic method in order to obtain the highest possible sensitivity per component. HCO_3^-, TOC and OMP analyses were performed by Het Waterlaboratorium.

The average values of the parameters – which were measured in duplicate or triplicate – are presented in the Results chapter. Deviations from the mean were indicated by error bars.

4

Results and discussion

4.1 Hydraulic permeability

Figure 8 depicts the clean water flux of a pristine dNF40 membrane at 20°C at various transmembrane pressures. The pure water permeability was found to be 5.8 $Lm^{-2}h^{-1}bar^{-1}$. In comparison, flat sheet NF membranes such as the NF270 have a pure water permeability of 13.6 $Lm^{-2}h^{-1}bar^{-1}$ (Hajibabania et al., 2011). The hydraulic permeability of the dNF40 falls in between commercial NF membranes and modern RO membranes with low water permeabilities of 1-2 $Lm^{-2}h^{-1}bar^{-1}$ (Te Brinke et al., 2020a).

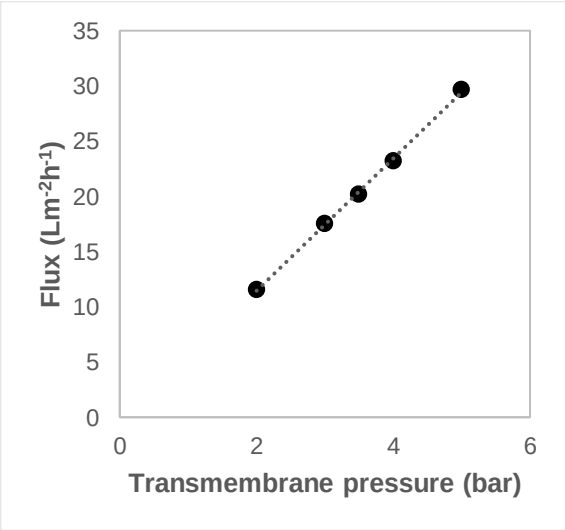

Figure 8. Clean water flux at different TMPs (cfv= 0.6 ms^{-1}; T=20°C).

The lower permeability of the dNF40 membrane is caused by the PEMs that decrease the pore sizes of the membrane. LbL coated PDADMAC/PSS membranes for example showed a clean water flux of 5 $Lm^{-2}h^{-1}bar^{-1}$ (De Grooth et al., 2015). Hydraulic permeability is dependent on the choice of polyelectrolyte and the number of multilayers applied. When 6 bilayers of PAH/PAA are deposited, a permeability of 1.8 $Lm^{-2}h^{-1}bar^{-1}$ was found due to the dense structure of the layers, while addition of a layer of PAH makes the PEMs swell and more permeable, resulting in a clean water flux of 3 $Lm^{-2}h^{-1}bar^{-1}$ (Ilyas et al., 2017). Membranes based on PAH/PSS show higher permeabilities of 13-16 $Lm^{-2}h^{-1}bar^{-1}$ (Te Brinke et al., 2020a). Recently it was discovered that asymmetric coated membranes have a high permeability of 12.8 $Lm^{-2}h^{-1}bar^{-1}$ while achieving exceptionally high OMP retention which outperforms commercial membranes (Te Brinke et al., 2020a). This new membrane category, the Chimera

membrane, was constructed by filling the support pores with an open PEM (PAH/PSS) and coating a thin layer of dense PEM (PAH/PAA) on top.

4.2 Molecular weight cut-off

The MWCO of the dNF40 membrane, the molecular weight above which 90% of the PEG molecules are retained, was found to be 214 Da or $gmol^{-1}$. The retention curve, where the MW of the PEGs is plotted against their retention, is shown in Figure 9. As larger molecules can potentially block the pores, this could lead to an overestimation of the MWCO. Therefore, also single PEG test with 200 and 300 Da were performed as control tests. Their measured MWCOs were 204 and 197 Da, respectively (the retention curves can be found in Appendix A). The supplier's estimated MWCO of 400 Da is thus a conservative estimate.

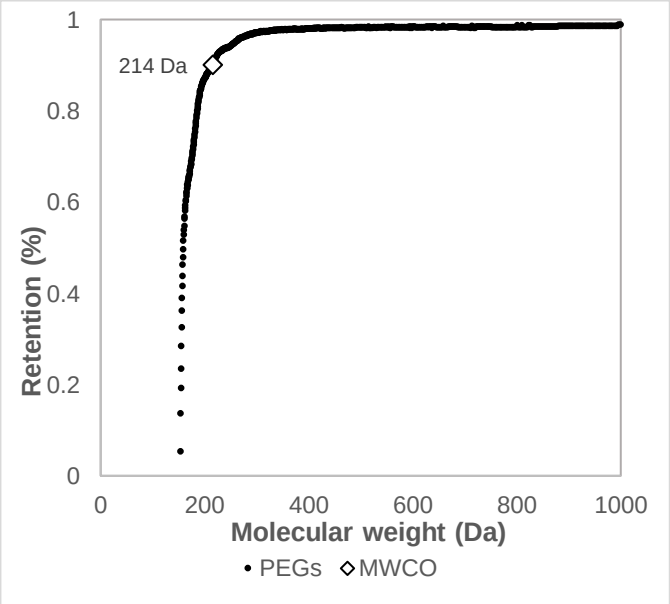

Figure 9. Determination of the molecular weight cut-off (MWCO) of the dNF40 membrane by filtration of PEG molecules (J=18 $Lm^{-2}h^{-1}$; cfv=0.6 ms^{-1}; T= 21°C).

The MWCO of the dNF40 membrane is comparable with dense NF membranes and almost borders the MWCO of RO membranes. In comparison: the flat sheet NF-90 and NF-200 membranes have a MWCO of ~200 and ~300 Da, respectively, while the ESPA2 RO membrane has a MWCO <200 Da (Yangali-Quintanilla et al., 2010). Hollow fiber NF membranes with PAH/PSS coating showed a MWCO of 301 $gmol^{-1}$, which dropped to 287 $gmol^{-1}$ when it was terminated with Nafion – both determined using PEG filtration (Reurink et al., 2019). The MWCO of asymmetric membranes was around 240 Da (Te Brinke et al., 2020a).

The radius of the pores of the dNF40 membrane was calculated to be 0.68 nm with equation (13) as stated in section 3.2.2. Pore sizes of flat sheet NF membranes are 1-10 nm and 0.5-1.5 nm for RO membranes (Wang et al., 2011).

4.3 Influence of Cl^- concentration on Cl^- retention

The retention of Cl^- at different feed concentrations, and the remaining concentrations in the permeate during filtration of SW are plotted in Figure 10. The Cl^- retention decreased with increasing Cl^- concentration. With an initial Cl^- value of 117 mgL^{-1}, the retention was 21.4%, leading to a permeate concentration of 92 mgL^{-1}. When the Cl concentration increased to 193 mgL^{-1} and 388 mgL^{-1}, only 19.0% and 16.2% of the Cl was retained, respectively. This results in permeate concentrations above the desired range of 80-90 mgL^{-1}.

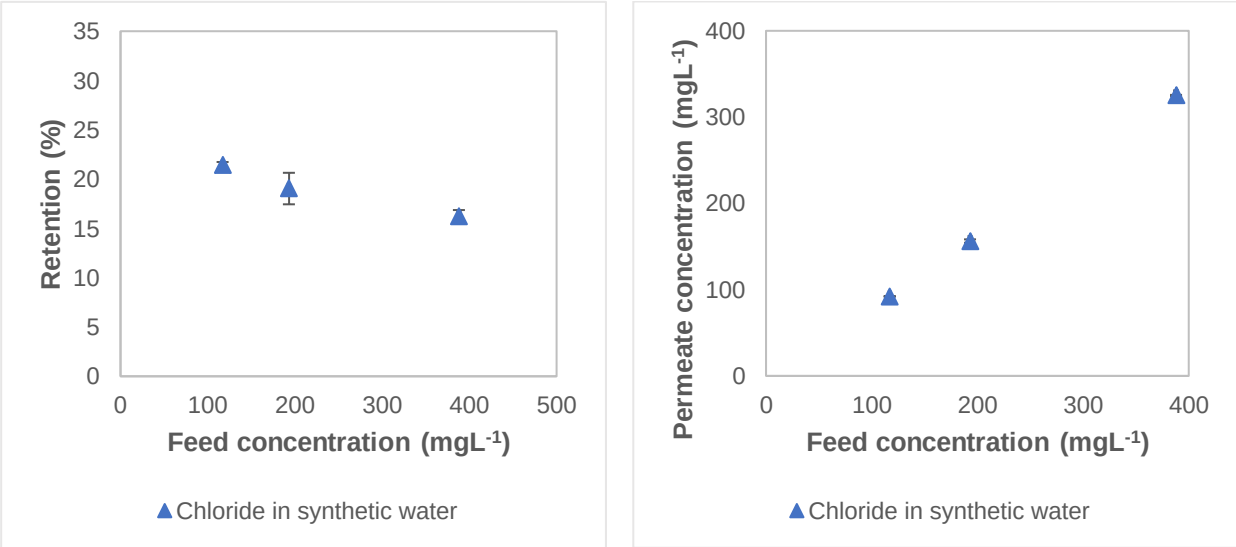

Figure 10. Retention of Cl^- (left) during increasing concentration in the feed and permeate concentrations (right) during dNF (cfv=0.6 ms^{-1}; J=18 $Lm^{-2}h^{-1}$; T=21°C).

The dependency of retention on Cl^- feed concentration was shown for negatively charged flat-sheet NF membranes, where a reduction in Cl^- retention could be observed with increasing NaCl concentration (Bandini et al., 2005; Wang et al., 2018). For LbL membranes, Cl^- retentions up to 91% have been reached with an 8-bilayer modified PDADMAC/PSS membrane at a feed concentration of 100 mgL^{-1} in the absence of other ions. When the feed concentration increased to 1000 mgL^{-1}, the retention dropped with 11% (Malaisamy et al., 2011). A reduction of Cl^- retention with the dNF40 membrane was thus expected with increasing concentration. This phenomenon has been attributed to the 'enhanced shielding effect' of the counterion Na^+ that can cause a reduction of the membrane surface potential, thereby reducing the electrostatic repulsion of the co-ion Cl^- (Bandini et al., 2005; Malaisamy et al., 2011; Wang et al., 2018).

4.4 Effect of cross-flow velocity on ion retention

Cross-flow velocities between 0.4-1.0 ms^{-1} were applied to determine the influence of cross-flow velocity on ion retention in SW. The results plotted in Figure 11 demonstrate that cross-flow velocity had a negligible effect on ion retention in SW, as only very small variations can be observed. The rejection by the membrane is primarily governed by the divalent ions, which is showed by 95.9% average retention for SO_4^{2-}, 84.7% for Mg^{2+} and 72.9% for Ca^{2+}. Furthermore, it can be observed that Mg^{2+} was better

retained than Ca^{2+} which in turn was better retained than Na^{+} (only 13.6%). These results are in line with previous research to LbL NF membranes (Cheng et al., 2018; Reurink et al., 2018). Very high rejections of SO_4^{2-} are known for negatively charged membranes (Costa & De Pinho, 2006; Ilyas et al., 2017; Abtahi et al., 2018), and the cation retention order of Mg^{2+} > Ca^{2+} > Na^{+} was shown by Cheng et al. (2018) for PDADMAC/PSS coated membranes, although they obtained lower cation retention values. With 21.5% retention on average, the retention of monovalent Cl^{-} in SW was much lower compared to its divalent co-ion. Earlier research already proved selectivity for Cl^{-} over F^{-} and SO_4^{2-} by PDADMAC/PSS coated membranes (Malaisamy et al., 2011).

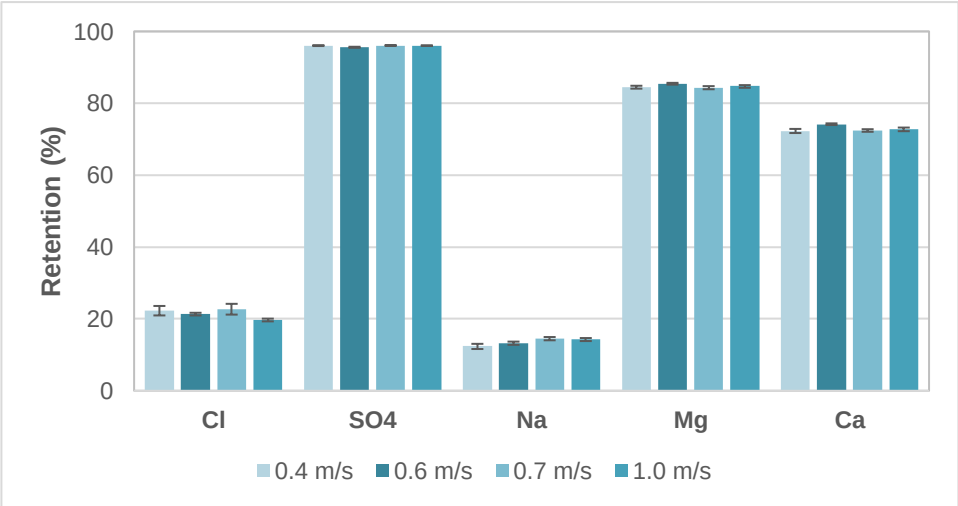

Figure 11. Retention of different ions during dNF of SW containing ~120 mgL^{-1} Cl^{-} (J=18 $Lm^{-2}h^{-1}$; T=21°C).

The rejection could be dominated by 'di-electric exclusion' (Ilyas et al., 2017), as the membrane is especially powerful in retaining multivalent charged species. The lower net charge of Cl^{-} affects Donnan (charge) exclusion as the monovalent Cl^{-} is less strongly repelled by the negatively charged membrane (Epsztein et al., 2018). Size exclusion could be an alternative explanation. Abtahi et al. (2018) indicated size exclusion followed by charge repulsion as the main mechanisms involved in salts retention by LbL membranes. The ion retention order in SW is in accordance with the order of their hydrated ion radii: SO_4^{2-} > Mg^{2+} > Ca^{2+} > Cl^{-} > Na^{+} (Kiriukhin & Collins, 2002; Cheng et al., 2018). Cheng et al. (2018) demonstrated that the retentions of Mg^{2+} and Ca^{2+} improved with the addition of bilayers, while high selectivity of Na^{+} remained. Considering the electrostatic attraction between the negatively charged membrane surface and cations, the higher divalent cation retention by the 5 bilayer PSS-terminated membrane was ascribed to 'increased size-exclusion effect'.

An increase of cross-flow velocity from 0.5-1.0 ms^{-1} showed to double the energy consumption with comparable salt retention (Jährig et al., 2018). However, higher fouling rates are expected when operating at low velocities, so the cross-flow velocity should not be chosen too low. For full scale NF plants, 0.2 ms^{-1} is commonly applied (Verliefde et al., 2008). In a previous lab-scale study to the dNF40 membrane, velocities above 0.5 ms^{-1} were recommended to sufficiently reduce concentration polarization (Arun, 2019). The manufacturer advices velocities of 0.2-0.4 ms^{-1} for full-scale applications.

4.5 Influence of permeate flux on ion retention

Figure 12 shows the rejection of different ions at different permeate fluxes during filtration of SW (in blue) and lake water from the VM (in green). Increasing permeate flux had a negligible effect on the retention of SO_4^{2-}, which was 95-96% in all cases with SW and even 98% with VM water. For the other measured ions applies that the retention increased with ascending flux. Higher permeate fluxes were achieved by increasing the pressure in the membrane element. Ion transport through the membrane includes diffusion, convection and electro-migration, and is dependent on the water flux, as shown in equation (1). When the solubility and diffusivity of the salts stay constant while the permeate water flux increases, the solute fluxes will decrease (Cheng et al., 2013). As long as the increase in water flux is larger than the increase in ion flux, the retention hence increases (Wang et al., 2014). Relatively many water molecules pass the membrane compared to ions, which dilutes the salt concentrations at the permeate side (Cheng et al., 2013).

Cl^- retention with SW increased from 20.5% at 11 $Lm^{-2}h^{-1}$ to 27.1% at 27 $Lm^{-2}h^{-1}$, leading to permeate concentrations of 95.1 and 86.7 mgL^{-1}, respectively. For VM water, Cl^- retention was considerably lower with only 8.9% at the highest applied flux, resulting in a permeate concentration of 212 mgL^{-1}, which is exceeding both the limit for infiltration water and the maximum allowed concentration in drinking water. HCO_3^- was only measured for VM water, showing 50.0% retention at 18 $Lm^{-2}h^{-1}$ and 53.0% at 28 $Lm^{-2}h^{-1}$, which led to concentrations around 116 mgL^{-1} in the permeate. Having sufficient HCO_3^- is desired as it functions as a buffer capacity and contributes to corrosion control (WHO, 2011).

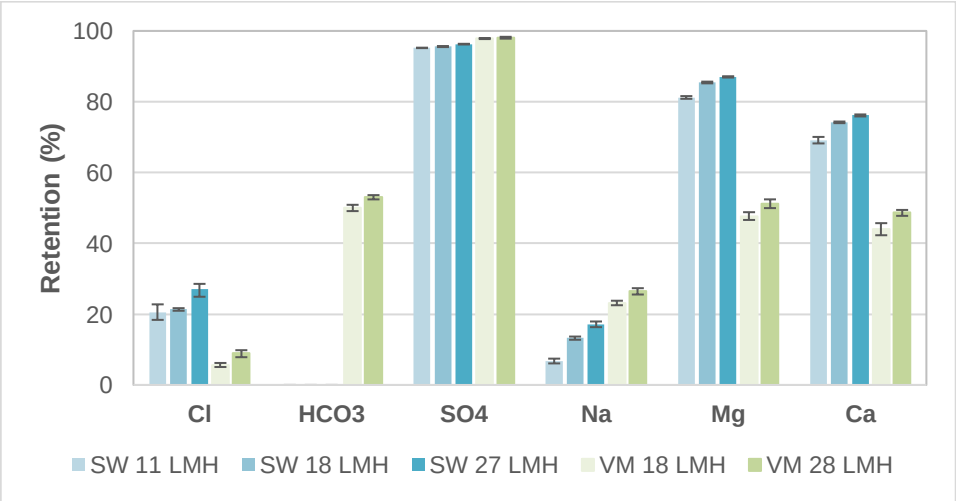

Figure 12. Retention of different ions during dNF of SW with ~120 mgL^{-1} Cl^- and VM water with ~230 mgL^{-1} Cl^- at varying permeate fluxes (cfv= 0.6 ms^{-1}; T=21°C).

For SW, Mg^{2+} was retained better than Ca^{2+} (81.2% compared to 69.1% at 11 $Lm^{-2}h^{-1}$), which in turn was retained much better than Na^+ (6.7%). Increasing the flux to 27 $Lm^{-2}h^{-1}$ resulted in 87.1%, 76.2% and 17.2% rejection of Mg^{2+}, Ca^{2+} and Na^+, respectively. Mg^{2+} retentions are known to be higher than Na^+ due to the difference in diffusivity (Tsuru et al., 1991). For VM water, cations were rejected in the same order as for SW: $Mg^{2+} > Ca^{2+} > Na^+$. However, Mg^{2+} was retained 38% less and Ca^{2+} 30% less

with VM water, while Na^+ showed 10% higher retention at 18 $Lm^{-2}h^{-1}$ than SW. The lower retentions for Mg^{2+} and Ca^{2+} might be caused by the presence of NOM in the VM water. The hampering effect of membrane fouling – indicated by substantial flux reduction – on membrane performance has been reported in previous research (Verliefde et al., 2009a; Yangali-Quintanilla et al., 2009; Sanches et al., 2012), but only a slight flux decline (<10%) was observed during the experiments. The negatively charged organic material could have adsorbed onto the polycation layers in the coating, which may have led to neutralization of the charge and made cation passage easier. However, a higher passage of Na^+ would then also be likely. Na^+ retention was not only higher with VM than with SW, it was also higher than Cl^- retention in VM water. A reversed order was expected due to the negative surface charge of the membrane. Nevertheless, SO_4^{2-} was well rejected and has to retain an equal charge of counterions. Mg^{2+} and Ca^{2+} were less strong retained than with SW, so more Na^+ was retained to balance and fulfil the electroneutrality principle.

4.6 Influence of system recovery on ion retention

In Figure 13, the Cl^- concentrations in the feed, the permeate collected at a specific recovery and the mixed permeate are shown at different system recoveries during filtration of both SW (in blue) and VM water (in green). Figure 14 depicts Cl^- retention while operating at a certain recovery value (triangles) and the average Cl^- retention (dots) at increasing system recovery for both water types. The Cl^- concentration in the synthetic feed water increased from initially 190 mgL^{-1} to 256 mgL^{-1} at 75% system recovery, leading to a concentration factor (CF) of 1.34. The Cl^- concentration in the VM feed water fluctuated around the initial value of 235 mgL^{-1} and hardly became more concentrated with increasing system recovery. For both water types, the Cl^- concentration in the permeate as well as in the mixed permeate increased with increasing system recovery, as shown by the rising permeate concentrations in Figure 13.

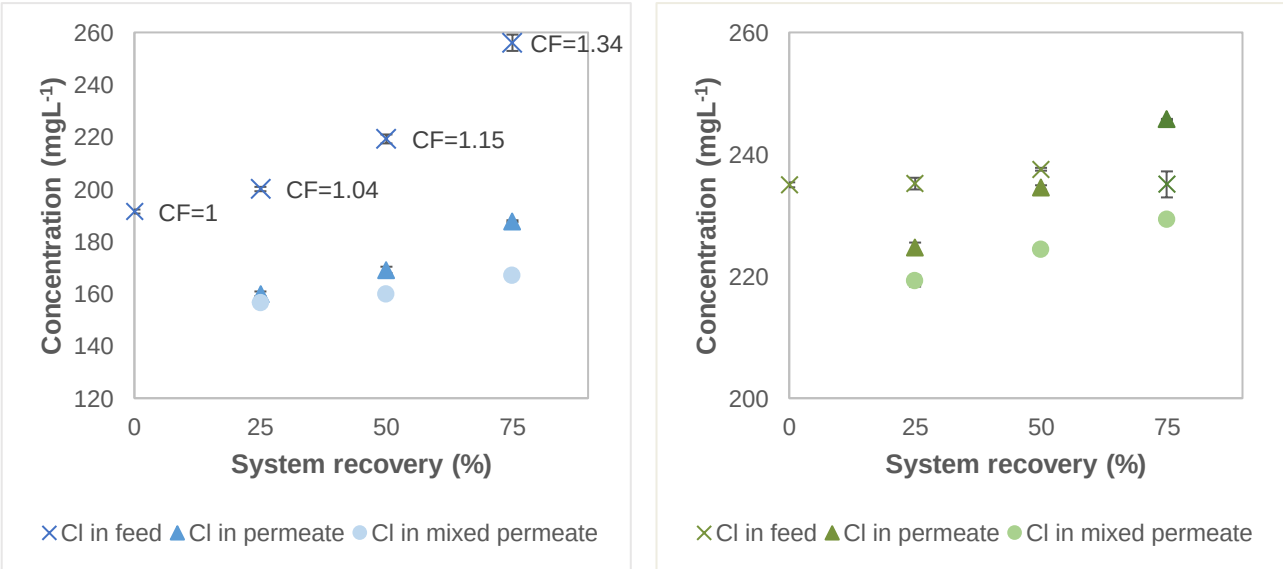

Figure 13. Cl^- concentration of the feed (crosses), permeate (triangles) and mixed permeate (dots) at different system recoveries during filtration of SW (left) and VM water (right) (J=18 $Lm^{-2}h^{-1}$; cfv=0.6 ms^{-1}; T=21°C). The concentration factor (CF) is shown with respect to the initial Cl^- concentration.

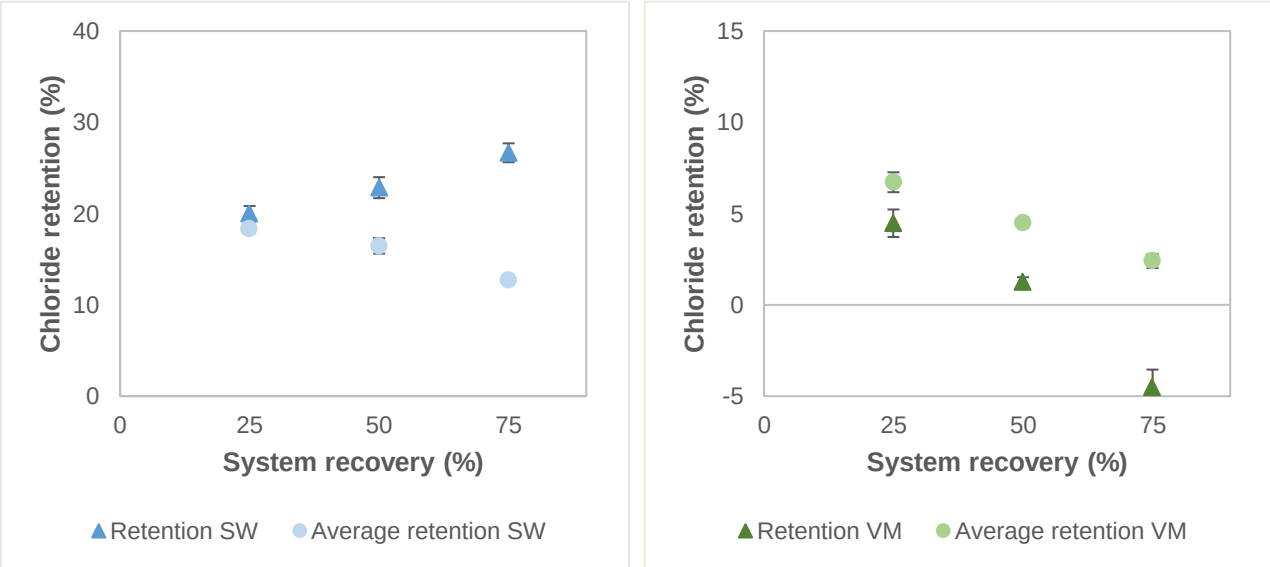

Figure 14. Cl^- retention with increasing system recovery during filtration of SW (left) and VM water (right). Retention (triangles) computed by concentration in permeate with respect to the concentration in the feed tank and average retention (dots) by concentration in mixed permeate with respect to the initial concentration.

From Figure 14 can be observed that the retention of Cl^- in SW with increasing system recovery increased percentage-wise due to the increasing CF, from 20.0% at 25% recovery to 26.7% at 75% recovery. However, in absolute values the permeate quality deteriorated as the feed water became more concentrated, which also led to higher Cl^- levels in the mixed permeate. Contrary to Cl^-, Na^+ retention in SW reduced with increasing system recovery, as represented in Figure 15.

For VM water can be noticed that the Cl^- retention decreased with increasing system recovery – while retention of SO_4^{2-} remained the same and retention of the cations Na^+, Mg^{2+} and Ca^{2+} increased with increasing system recovery, as can be seen in Figure 15. Interestingly, negative retention of Cl^- (-4.5%) was observed while filtrating real lake water at 75% system recovery. In the produced permeate, 246 mgL^{-1} of Cl^- was detected, which was higher than the concentration in the feed water (235 mgL^{-1}).This negative retention probably occurred as a result of the strong rejection of SO_4^{2-}, which was present in high concentrations and is in competition with other negatively charged compounds (Verliefde et al., 2009a; Ilyas et al., 2017). Due to the Donnan effect, the multivalent anions are rejected at the expense of the monovalent Cl^- ions because of their stronger valence (Tsuru et al., 1991). The negative retention of Cl^- can be explained by the Nerst-Planck equation as stated in equation (1). Relatively many Cl^- ions pass the membrane with respect to the number of water molecules – i.e. the ion flux is high compared to the water flux –, causing a higher Cl^- concentration in the permeate than in the feed water (Cheng et al., 2013).

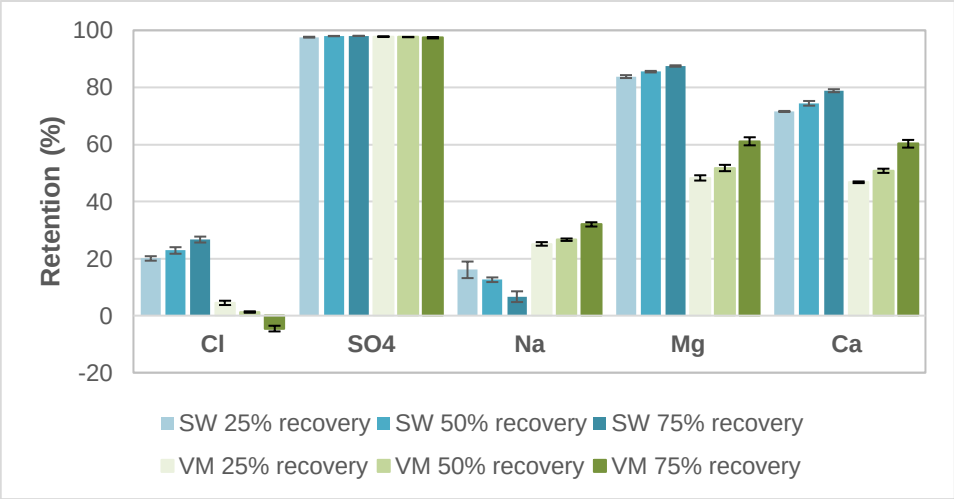

Figure 15. Retention of different ions during filtration of SW (blue) and VM water (green) at 25%, 50% and 75% system recovery (J=18 $Lm^{-2}h^{-1}$; cfv=0.6 ms^{-1}; T=21°C).

At high recovery, the SO_4^{2-} concentration increased to almost four times the initial concentration, but the retention remained high: 98.0% at 75% recovery with an average retention of 96.1% in case of SW. The same trend occurred with filtration of VM water, where the retention was 97.4% at 75% recovery with an average retention of 95.8%. At 75% recovery, the feed water contained 359 mgL^{-1} SO_4^{2-} in VM water and 261 mgL^{-1} SO_4^{2-} in SW. High SO_4^{2-} retention is known for (LbL) NF membranes (Verliefde et al., 2009a; Ilyas et al., 2017; Abtahi et al., 2018; Reurink et al., 2018; Reurink et al., 2019).

Overall, the quality of the mixed permeate decreased when reaching higher system recoveries for both water types. The mixed permeate of SW showed an average Cl^- retention of 18.3% at 25% recovery, 16.5% at 50% recovery and 12.7% at 75% recovery, the latter resulting in a mixed permeate concentration of 167 mgL^{-1}. In case of filtration of VM water, the average Cl^- retention diminished from 6.7% at 25% recovery to 2.4% at 75% recovery. This led to a Cl^- concentration of 229 mgL^{-1} in the mixed permeate, which is far above the desired range. The average ion retention at 75% system recovery is 29.9% for SW and 20.8% for VM water at 75% recovery.

4.7 Performance towards OMPs

For SW, retention values of the spiked OMPs were compared after 24 and 48 hours of filtration, as it takes some time to reach membrane saturation. The average OMP rejection of 88.1% after 24h of contact time with SW increased to 89.0% after >48h of contact time, indicating that the membrane surface was already saturated after 24h of recirculation. With lake water, the average rejection dropped to 79.0%. Retention values of all different components during filtration of both water types are depicted in Appendix B.

Sulfamethoxazole (253 $gmol^{-1}$), a negatively charged compound with a molecular weight close to the MWCO, was retained with 95.4% in SW, which is in line with findings of Te Brinke et al. (2020a). With the hollow fiber Chimera membrane, they obtained up to 96% retention of sulfamethoxazole spiked in

demi water. The retention with the dNF40 membrane is ~40% higher than retention with the NF270 membrane (Chang et al., 2012) and ~35% higher than with the NF200 membrane (Yangali-Quintanilla et al., 2009). For filtration of VM water, the retention decreased to 90.9%.

The retention of the negatively charged diclofenac (296 $gmol^{-1}$) was 98.1% versus 96.9% for SW and VM water, respectively. These values approach diclofenac retentions of 99-100% of commercial NF membranes (Abtahi et al., 2018). With a PAH/PAA coated hollow fiber membrane, up to 77% diclofenac removal from synthetic wastewater was reached (Abtahi et al., 2018). Despite the negative charge of diclofenac, size exclusion was indicated as the dominant mechanism of OMP removal with this LbL membrane.

From Figure 16 it can be observed that the retention values for negatively charged pharmaceuticals (97.2% for SW compared to 94.7% for VM) were higher than the values for positively charged compounds (92.0% for SW versus 79.3% for VM), which in turn were higher than those of neutral pharmaceuticals (72.6% for SW compared to 56.5% for VM). A retention order of negatively charged > neutral > positively charged was however demonstrated by Verliefde et al. (2008) with negatively charged NF membranes. The difference in retention order could be explained by the LbL structure of the dNF40 membrane where underlying polycation layers can promote the repulsion of positively charged OMPs (Reurink et al., 2019). Some types of polycation are excessively present inside the multilayers and tend to overcompensate, thereby creating surplus positive charge (Reurink et al., 2018; Reurink et al., 2019). De Grooth et al. (2014) also found a rejection order of negatively charged OMPs > positively charged OMPs > neutral OMPs for negatively terminated LbL membranes. The high retention of negatively charged compounds was attributed to the charge repulsion of the membrane, which is comparable to the high SO_4^{2-} retention.

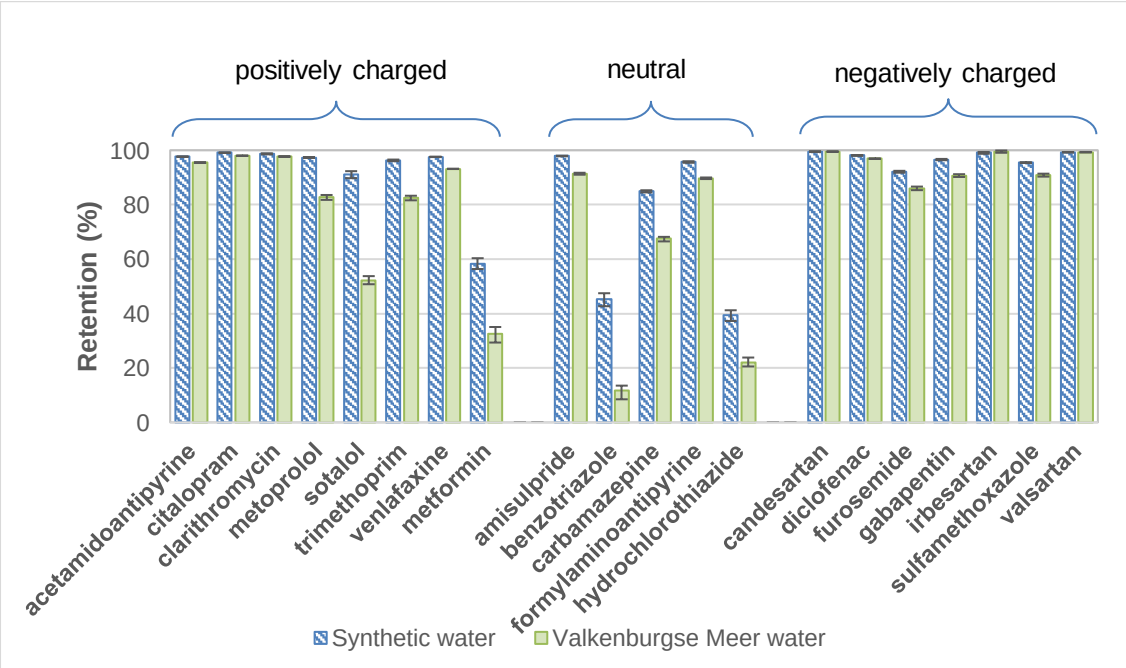

Figure 16. Rejection of selected pharmaceuticals in synthetic and real surface water at pH 8.

The high retention of negatively charged compounds can be explained by electrostatic interactions between the pharmaceuticals and the negatively charged membrane surface (De Grooth et al., 2014). The positively charged OMPs are attracted towards the oppositely charged membrane which causes an increased concentration of positively charged compounds at the membrane surface in comparison to the feed solution, also known as 'concentration polarization' (Verliefde et al., 2008). A part of the solutes diffuses to the permeate side, resulting in lower retentions. For neutral pharmaceuticals, no charge interactions with the membrane occur, so smaller compounds can more easily pass the membrane.

The retention differences between SW and VM were on average much bigger for positively charged compounds (12.7%) and neutral pharmaceuticals (16.2%) than for negatively charged compounds (2.5%). The largest difference between the two water types is the presence of 11.6 mgL^{-1} of natural organic matter (measured as TOC) in VM water. Deposition of negatively charged NOM on the membrane surface possibly leads to an increased negative surface charge (Verliefde et al., 2008). This could explain the smaller difference in rejection of negatively charged OMPs in SW and VM water in comparison to neutral or positively charged compounds. The increased negative surface charge could possibly result in a decrease in the retention of positively charged OMPs. Deposition of negatively charged NOM on the membrane surface would however only explain the lower observed rejection values for positively charged OMPs (Verliefde et al., 2007b), and not the large difference for neutral OMPs.

The majority of OMPs with a molecular weight above the MWCO showed >90% retention in SW and >80% in VM water, except for three components. Hydrochlorothiazide (298 $gmol^{-1}$) was retained with 39.3% and 22.1% retention in SW and VM water, respectively. Sotalol (272 $gmol^{-1}$) was retained by 91.1% in SW but with only 52.2% retention in VM water, which is a remarkable difference. These two compounds are hydrophilic as can be derived from their log D values which are presented in Table 6. These polar compounds dissolve very well in water, which complicates their removal. Carbamazepine (236 $gmol^{-1}$) showed 84.9% retention in SW compared to 67.5% in VM water. This is a slightly hydrophobic compound. In Figure 17, the retention of six OMPs that showed deviant behavior are plotted against their molecular weight.

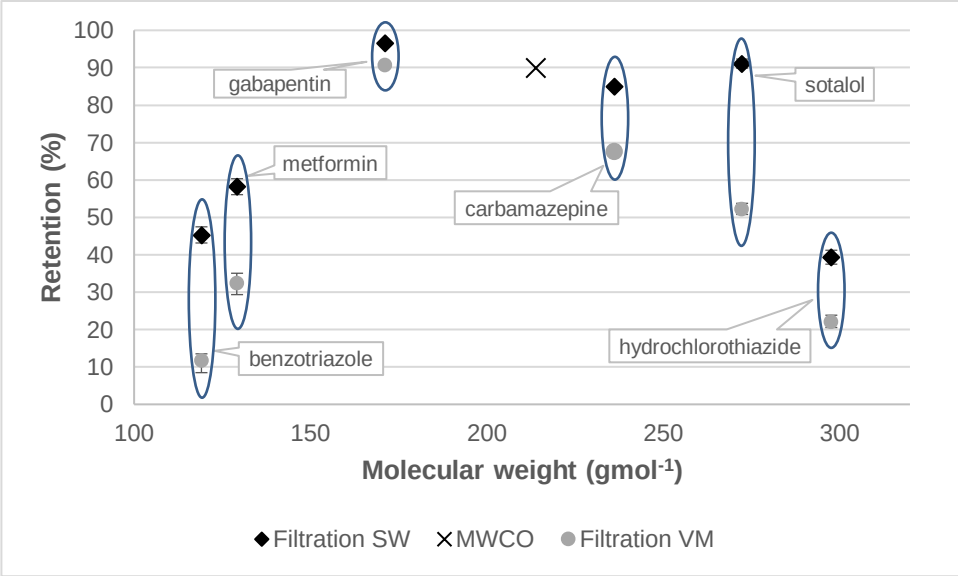

Figure 17. Deviating retention of six OMPs by the dNF40 membrane as a function of molecular weight and feed water type.

Notable is the high retention of gabapentin (171 $gmol^{-1}$) – 96.6% in SW and 90.7% in VM – while this component is smaller than the MWCO. This is beneficial as gabapentin is known to be poorly biodegradable under anaerobic conditions and thus no significant degradation during dune passage is expected (Henning et al., 2018). The two other components which were smaller than the MWCO, metformin (129 $gmol^{-1}$) and benzotriazole (119 $gmol^{-1}$), were however not so well rejected. All three compounds are hydrophilic and therefore dissolve well in water. The higher rejection of gabapentin could be dedicated to its negative charge which is repulsed by the negatively charged membrane surface. Metformin, a positively charged component, was slightly retained better than the neutral benzotriazole. Benzotriazole was proven to be hardly degraded during soil passage. However, the compound is removed to high extend in the post-treatment by addition of PAC (Reemtsma et al., 2010).

Metformin is used in enormous quantities as anti-diabetic and ends up in recipient waters such as the rivers Meuse and Rhine in the range of μgL^{-1}, despite the fact that this compound is converted for >90% by bacterial degradation in sewage water treatment plants (Scheurer et al., 2009; Houtman et al., 2014). In the middle of the VM, 0.14 μgL^{-1} was detected on 20 August 2020. The retention of spiked metformin (129 $gmol^{-1}$) was 58.2% in SW and 32.5% in VM water, which is poor but slightly higher than with advanced oxidation – about 20-25% conversion was reached with O_3/H_2O_2 (Knol et al., 2015). Furthermore, flocculation and activated carbon filtration have proven to be ineffective for removal of metformin, but soil passage showed almost complete removal of this compound (Scheurer et al., 2012). Therefore, it is likely that the remaining metformin in the infiltration water will degrade during dune passage.

Table 6. Structure and physico-chemical characteristics of six deviating OMPs.

Compound		MW ($gmol^{-1}$)	pKa (-)	charge	log K_{ow} (-)	log $D_{(pH\ 8)}$ (-)
benzotriazole	$C_6H_5N_3$	119	8.2	0	1.44	1.15
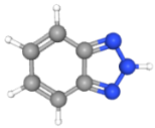						
carbamazepine	$C_{15}H_{12}N_2O$	236	15.96	0	2.45	2.45
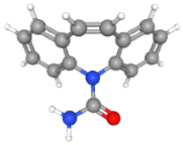						
gabapentin	$C_9H_{17}NO_2$	171	4.63	–	-1.1	-1.10
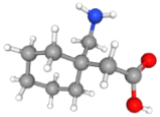						
hydrochlorothiazide	$C_7H_8ClN_3O_4S_2$	298	9.09	0	-0.07	-0.13
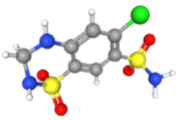						
sotalol	$C_{12}H_{20}N_2O_3S$	272	10.07	+	0.24	0.23
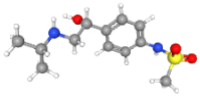						
metformin	$C_4H_{11}N_5$	129	12.33	+	-2.64	-2.64
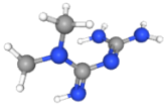						

The retention of pharmaceuticals was on average 10% lower in VM water than in SW, but the biggest deviation could be observed with benzotriazole (34% less) and sotalol (39% less). The lower retention of benzotriazole in VM water than in SW could have been affected by the feed concentration, which was more than twice as high in VM water as in SW. Differences in ionic strength could be another influencing factor. In a previous research was shown that with increasing ionic strength, the retention of NOM increased but the retention of the studied OMP decreased (Devitt et al., 1998). Although VM water had a slightly higher NaCl content than SW, their ionic strengths were comparable. For the removal of pesticides with spiral wound NF membranes it was shown that the molecular length has a significant influence on retention (Chen et al., 2004). This relationship could however not be found in this study. More research is thus required to explain the retention differences.

4.8 Comparison of effluent at 75% system recovery with requirements for infiltration water

In Table 7, the quality of the mixed permeate at 75% system recovery is shown of both SW and VM water in comparison with Dunea standards for infiltration water and the legal standard. The so-called 'Infiltratiebesluit' originates from 20 April 1993 and contains rules with regard to the infiltration of water obtained from surface water into the soil. The company standards of Dunea are based on the P_{99} values of the water that is infiltrated at Meijendel and only apply to water that is infiltrated into the dunes (Van Altena, 2017). The legal drinking water standards of the 'Drinkwaterbesluit' (from 10 October 2010 onwards) are also shown below. For OMPs there are no legal standards yet for drinking water or drinking water sources, but a signaling value of 1 μgL^{-1} has been included (Moermond et al., 2016). For new emerging contaminants of which the effects are still unknown, a precautionary value of 0.1 μgL^{-1} applies.

Table 7. Comparison of parameters of interest of SW and VM water at 75% system recovery with requirements for infiltration water. The values of Dunea and legal standards are the maximum desired and allowed values. Values exceeding the maxima of the legal standard are indicated in red.

Parameter	SW	VM water	Dunea standards	Infiltratie-besluit	Drinkwater-besluit	unit
pH	8.25	8.19	8.25		7.8-8.5	-
EC	767	990	566		<1000	μScm^{-1}
turbidity	<0.03	0.18	0.82		<1	NTU
hardness	0.81	1.79	2.11		1-2.5	$mmolL^{-1}$
TOC	<1.83	0.31	4.68			mgL^{-1}
NO_3^-	<2.79	1.61	16.12	<24.8	<50	mgL^{-1}
NH_4^+	<0.02	<d.l.	0.8	<3.2	<0.5	mgL^{-1}
PO_4^{3-}	<0.13	<d.l.	0.21	<1		mgL^{-1}
Na^+	121.4	124.4	44.8	<120	<150	mgL^{-1}
K^+	5.27	12.2	7.09			mgL^{-1}
Mg^{2+}	3.94	14.4	9.5			mgL^{-1}
Ca^{2+}	25.9	47.4	71.1			mgL^{-1}
F^-	<0.22	<d.l.	0.28	<1		mgL^{-1}
Cl^-	167	229	73.4	<200	<150	mgL^{-1}
Br^-	<d.l.	<d.l.	0.14			mgL^{-1}
HCO_3^-	?	169	211		>60	mgL^{-1}
SO_4^{2-}	2.64	3.53	60.6	<150	<150	mgL^{-1}
Ion balance	-6.58	-0.00				%

After filtration, most parameters meet the legal standards for infiltration, except for Na^+ in both water types and Cl^- in case of filtration of VM water. It should be considered that in the traditional post-treatment after dune passage, these compounds are not further reduced. Additional treatment is therefore required to meet the standards of the 'Infiltratiebesluit' but also to meet the drinking water

standard for Cl^- and Na^+ of <150 mgL^{-1}. In Chapter 5, different options to obtain the desired water quality for dune infiltration are discussed.

The raw VM water contained relatively high levels of Mg^{2+} and Ca^{2+}, which causes hardness. Hard water leads to higher soap consumption and can cause scaling in the water distribution system and heated water applications (WHO, 2010). Therefore, softening is often an applied treatment step in drinking water treatment plants. With hollow fiber NF as pretreatment, scale-forming ions such as Mg^{2+} and Ca^{2+} are removed to a large extend. The filtrated SW showed a hardness below 1 $mmolL^{-1}$, which is a bit too low as some hardness is required to prevent water from becoming aggressive (WHO, 2010). Filtration of VM water at 75% system recovery resulted in a hardness of 1.79 $mmolL^{-1}$, which complies with the drinking water standards. As a result, the softening step in the post-treatment might (partially) become unnecessary, saving space, energy, materials and costs.

Dissolved minerals do not only influence corrosion or scaling processes, but they also contribute to the taste of drinking water (WHO, 2010). Demineralized water tends to have a flat taste, so producers of bottled demineralized water often add ions such as HCO_3^-. In case of direct NF, a part of the HCO_3^- was removed from the VM water, but sufficient remained to meet the standard of >60 mgL^{-1} for drinking water.

Considering the average Cl^- concentrations in the VM from 2016 to 2020 (depicted in Table 8), the measured values of ~235 mgL^{-1} were much higher than expected. This is probably the result of a dry summer in combination with the interference of the Wassenaarse Watering, where Cl^- levels even exceeded 1300 mgL^{-1} this summer due to temporary discharge of brackish groundwater to the canal. The Cl^- concentration in the Wassenaarse Watering is usually below 100 mgL^{-1} (Zwolsman et al., 2019). Nevertheless, over the past years an increasing trend in Cl^- concentration in the VM can be observed and should be taken into account in the conceptual design.

Table 8. Average Cl^- concentrations from 2016-2020 in the VM.

Cl (mgL^{-1})	Q1	Q2	Q3	Q4	Yearly average
2016	123	117	110	117	117
2017	118	120	123	121	121
2018	117	120	134	137	127
2019	142	144	159	150	149
2020	151	152	171		156

5

Conceptual design

5.1 A full-scale dNF40 plant for pretreatment location Katwijk

In total, 32 million m^3y^{-1} can be abstracted from the VM. The NX Filtration Projection Tool v2.04i was used to calculate the required number of modules to achieve a certain permeate flow. The tool was also used to predict the permeate water quality produced with the selected WRC200-dNF40-IRD membrane module at higher system recoveries. Below, a comparison of a full-scale dNF40 plant operating at 75% and 85% system recovery is shown. Two scenarios were used in the projection: a winter scenario (with 143 mgL^{-1} Cl^- at 5°C) and a summer scenario (235 mgL^{-1} Cl^- at 20°C). The complete water composition of both scenarios can be found in Appendix C.

Table 9. Comparison of the designs of a full-scale dNF plant for Katwijk operating at 75% and 85% system recovery in summer and winter period based on the projection tool.

Recovery (%)	T (°C)	feed pressure (bar)	total # of modules	Cl in feed (mgL^{-1})	Cl in mixed permeate (mgL^{-1})	Cl retention (%)	energy requirement ($kWh.m^{-3}$)
75	20	4.83		235	203	13.6	
	5	7.85		143	123	14.0	
			2664				**0.40**
85	20	4.84		235	212	9.8	
	5	7.85		143	129	9.8	
			3024				**0.37**

The projection tool predicted an overall Cl^- retention of 13.6% for the full-scale modules, while only 2.4% was achieved with the in the lab-scale unit. From Table 9 can be seen that operation at lower water temperatures required higher pressures due to the lower viscosity of the water. The Cl^- retention was roughly 10% at 85% system recovery, independent of the summer or winter scenario. Higher recovery means more permeate produced and less energy consumed per produced cubic meter. With a salinity below 2000 ppm, the produced concentrate is only slightly brackish. For the conceptual design of the pretreatment in Katwijk, the projection of the summer scenario at 85% system recovery was selected. With the applied pressures, an average membrane flux of 20.5 $Lm^{-2}h^{-1}$ can be reached. A cross-flow velocity of 0.2 ms^{-1} was applied, which is a common cross-flow velocity in full-scale NF plants (Verliefde et al., 2007a). This low velocity results reduces energy consumption, which was estimated to be 0.37

$kWhm^{-3}$. Jährig et al. (2018) estimated the specific energy consumption of hollow fiber NF in the same range.

The selectivity for the passage of monovalent ions over divalent ones of LbL NF membranes makes high fluxes and energy efficiency possible. However, for the purpose of Dunea, not sufficient Cl^- is removed at higher system recoveries. To comply with the directives of the 'Infiltratiebesluit' and the company standards, additional (or adaptational) steps are thus required in order to obtain a water quality that meets the standards. Below, four options are mentioned which could be suitable solutions.

1. **Modification of the membrane**: creating a slightly denser membrane by additional PEMs to the dNF40 membrane or a different type of coating potentially increases Cl^- retention. The biggest advantage of this solution is that the pretreatment of VM water can still consist of a single step.
2. **Side stream RO**: to reduce Na^+ and Cl^- levels, partial RO treatment of the dNF40 treated water is an option. For efficiently operating membrane desalination, inorganic scaling is a major obstacle (Cheng et al., 2018). It was however shown that the dNF40 membrane successfully removed scale-forming divalent cations, resulting in a direct applicable feed stream for RO. The drawbacks of a side stream RO are however the costs and the removal of all ions while only NaCl has to be reduced. This scenario is elaborated in section 5.3.1.
3. **Electrodialysis reversal (EDR)**: 'mild desalination' can be achieved by EDR as this technique can selectively extract ions from a solution (Gärtner et al., 2005). In the process, an electrical potential gradient across a stack of alternating cation and anion exchange membranes is used (Bisselink et al., 2016). However, Yen et al. (2017) compared RO and EDR as final treatment step in the wastewater reclamation process and concluded that RO can provide a higher desalination rate at lower treatment costs.
4. **Mixing with Meuse water**: another way to reduce the NaCl content is to mix the dNF40 water with pretreated Meuse water, which has a Cl^- concentration of ~60 mgL^{-1}. The VM could then not only be used as a source for Katwijk, but also for Scheveningen and Monster, thereby decreasing the demand of the current pretreatment in Bergambacht and most importantly: this scenario would decrease the pressure on the on the transportation pipes even more as less water needs to be transported. This scenario is further elaborated in section 5.3.2.

5.2 Visual impressions of the dNF plant

In total, 32 million m^3y^{-1} can be abstracted from the VM. The extracted 3653 m^3h^{-1} is divided over 12 treatment lanes, which results in a flow of 305 m^3h^{-1} per train. This is a practical design choice based on a maximum skid design of 84 elements that can be placed in parallel while being powered by one pump. The plant operates in so-called feed-and-bleed mode, where a part of the concentrate is recirculated over the membrane to increase module recovery. Furthermore, a multi-stage configuration is applied in order to obtain higher system recoveries. The collected concentrate of the first stage forms the feed water for the second stage, and so on (depicted in Figure 19). In total, three stages are required

to obtain a system recovery between 75-85%. In the configuration with 85% system recovery, 84 elements are required per stage, resulting in 252 elements per treatment street and a total requirement of 3024 elements. The recovery of the first, second and third stage are 28.5%, 39.7% and 65.1%, respectively. This implies that 87 m^3h^{-1} of permeate is produced per stage, leading to 259 m^3h^{-1} per lane and hence 3109 m^3h^{-1} in total. Cleaning cycles were included in the projection. The membranes are cleaned hydraulically by means of forward flush every 4 hours (based on empirical findings); chemical cleaning is applied once every week.

In Figure 18, a visual impression of a single stage in one of the treatment streets is depicted. In Figure 20, a complete overview of the dNF plant is presented. The visuals were created in MicroStation with support from Blaauw Bloed. An area of 70 m by 40 m is minimally required for installation of the elements and pipes. Furthermore, the building to be constructed should have a minimum height of 4 m. The proposed location for the dNF40 plant at treatment facility Katwijk is represented in Figure 21.

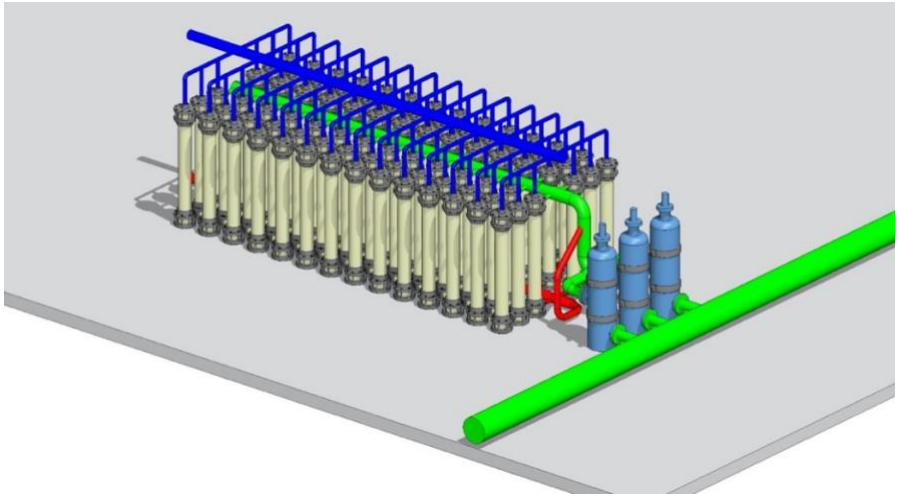

Figure 18. Visual impression of a single dNF stage with 84 modules within one treatment lane, preceded by three 100-micron strainers.

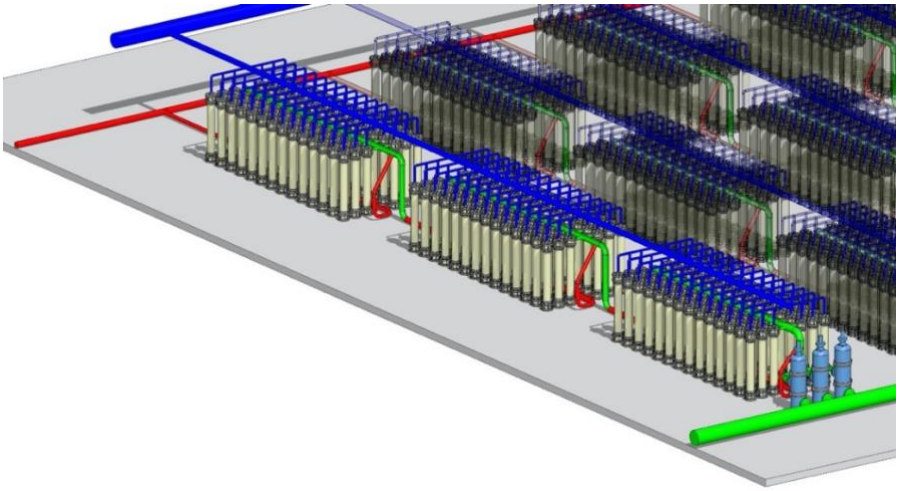

Figure 19. Visual impression of a treatment lane consisting of three stages, where the concentrate of the first stage continues as feed water for the second stage. All produced permeate is collected separately.

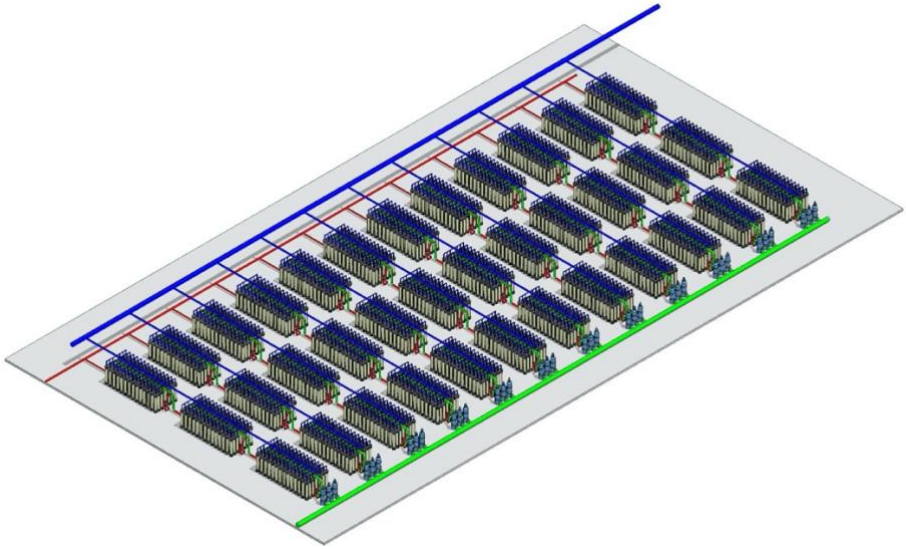

Figure 20. Overview of the dNF plant Katwijk with 12 treatment lanes for the treatment of 32 million m^3y^{-1} from the VM.

Figure 21. Location of the dNF40 plant in Katwijk.

5.3 Elaboration of the scenarios

5.3.1 Side stream RO

After dNF treatment, the water still contains 212 mgL^{-1} Cl^- in summer and 129 mgL^{-1} in winter. In this section, the second proposed solution is further elaborated. When desiring a Cl^- concentration of at least below 100 mgL^{-1} throughout the year, a side stream RO treatment of 55% is required in summer while in winter time, only 25% side stream is necessary. In total, 3653 m^3h^{-1} can be abstracted from the VM. At a recovery of 85%, hence 3109 m^3h^{-1} of permeate is produced. This implies that 1710 m^3h^{-1} and 777 m^3h^{-1} have to be treated by RO in summer and winter, respectively. In Figure 22, the process flow diagram is presented, including the hydraulic line.

The pretreatment plant will be built at the site of Dunea's posttreatment location of Katwijk as there is sufficient space available. From the intake point (-1 m below the water surface) at the north-east corner of the lake, the water needs to be transported over a distance of 4.1 km (Kraaijeveld et al., 2020) and should overcome an elevation difference of ~9 m (determined from Actueel Hoogtebestand Nederland). The route of the pipeline is presented in Appendix C. The diameter of the abstraction pipe was computed to be 1.2 m using a velocity of 0.9 ms^{-1}. All head losses during transportation due to wall friction were computed using Darcy-Weisbach's equation in terms of the volumetric flow Q:

$$\Delta P_H = \lambda \cdot L \cdot \frac{8}{\pi^2 g} \cdot \frac{Q^2}{d^5} \quad (14)$$

In the calculations, the friction factor was assumed to be 0.02. In total, 9 m + 3 m (head loss) = 12 m head is required to pump the water from the lake to the pretreatment location. Here, the flow is divided over 12 lanes. Per lane, three 6" Amiad Sigma Pro filters of 100 micron with a capacity of 50-180 m^3h^{-1} are installed in parallel (only two are operational), requiring minimally 1.5 bar. The head losses over these filters are roughly 1 m at a flow of about 150 m^3h^{-1} (Amiad, 2020). The dNF installation requires a feed pressure of 4.84 bar (and up to 7.85 bar in winter), so the pumps should at least be able to provide 50 m head. The head loss over the hollow fiber membrane modules is about 2 m. The concentrate has a pressure of 4.65 bar in summer and 7.57 bar in winter, while the permeate has no pressure. From the mixing tank the water thus has to be pumped to the infiltration site.

With 85% recovery of the dNF plant and 90% recovery of the RO treatment, in total 26.1 million m^3 of infiltration water can be produced per year with this pretreatment configuration. The combined concentrate from the dNF treatment and side stream RO is relatively fresh – a stream of approximately 704 m^3h^{-1} with 747 mgL^{-1} of Cl^- in summer and 620 m^3h^{-1} with 468 mgL^{-1} of Cl^- in winter is produced. However, it is undesirable to discharge the concentrate to surrounding surface waters, so the most promising solution for concentrate disposal would be discharge into the sea. Drinking water company PWN also discharges its RO concentrate on the North Sea, which could be beneficial for the application of a permit (Zwolsman et al., 2019). The concentrate contains enough pressure to be transported to the

North Sea without the requirement of a pump. The suggested route for this pipeline towards the sea is shown in Appendix C.

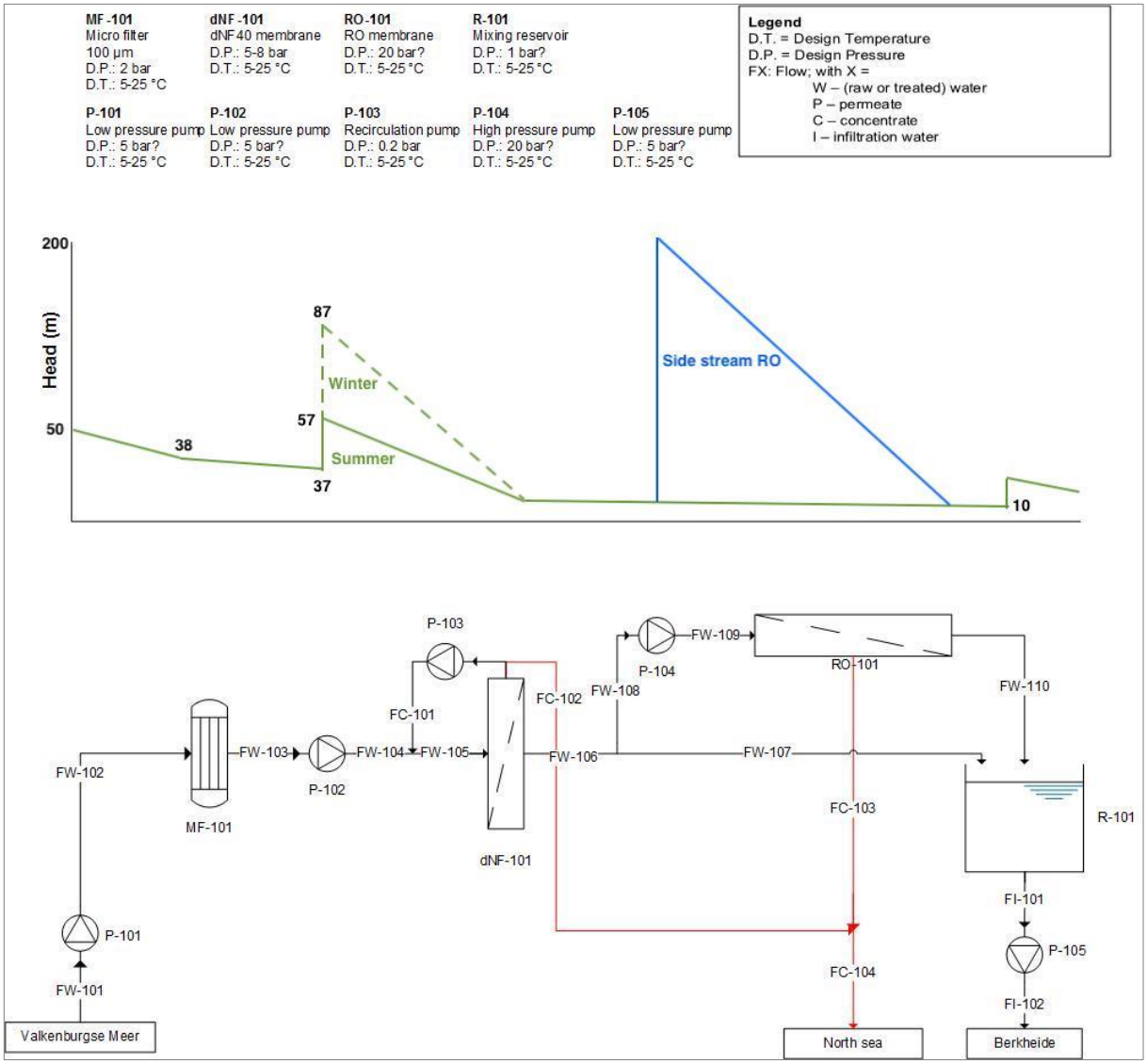

Figure 22. Process flow diagram (PFD) and hydraulic line of dNF plant with side stream RO treatment.

5.3.2 Mixing with Meuse water

The complete water demand of the Katwijk region could be taken over by the VM as source in terms of quantity. However, the required side stream RO treatment to comply with infiltration standards might not be desirable due to the higher investment costs, larger energy requirement and additional footprint. Another option to reduce the NaCl concentration is to mix the dNF40 water with pretreated Meuse water. Exploiting the full capacity of the afore designed dNF40 plant, more infiltration water can be produced in the mixing scenario than for the infiltration sites of Berkheide alone: the surplus water capacity of pumping station Katwijk can be transported to the infiltration sites of Meijendel (Scheveningen) and Solleveld (Monster). This scenario builds towards a more robust and resilient water treatment strategy. Although the disadvantage of the long transportation distance from Bergambacht to the dune area remains, less water has to be taken in from the Afgedamde Maas for infiltration water production for Meijendel and Solleveld as well, thereby relieving the pressure on the entire current system. This will also result in lower losses due to leakages.

The infiltration water originating from the Meuse shows average concentrations of ~60 mgL^{-1} Cl^-, ~40 mgL^{-1} Na^+, ~9 mgL^{-1} Mg^{2+} and ~60 mgL^{-1} Ca^{2+}. During dune passage, no changes in concentrations of Cl^-, Na^+ and Mg^{2+} take place, but Ca^{2+} is added to the water due to dissolution of shells. The abstracted water contains ~70 mgL^{-1} Ca^{2+}. In Figure 23, both the concentrations of the 4 mentioned ions in the infiltration water and in the abstracted water after dune passage are depicted.

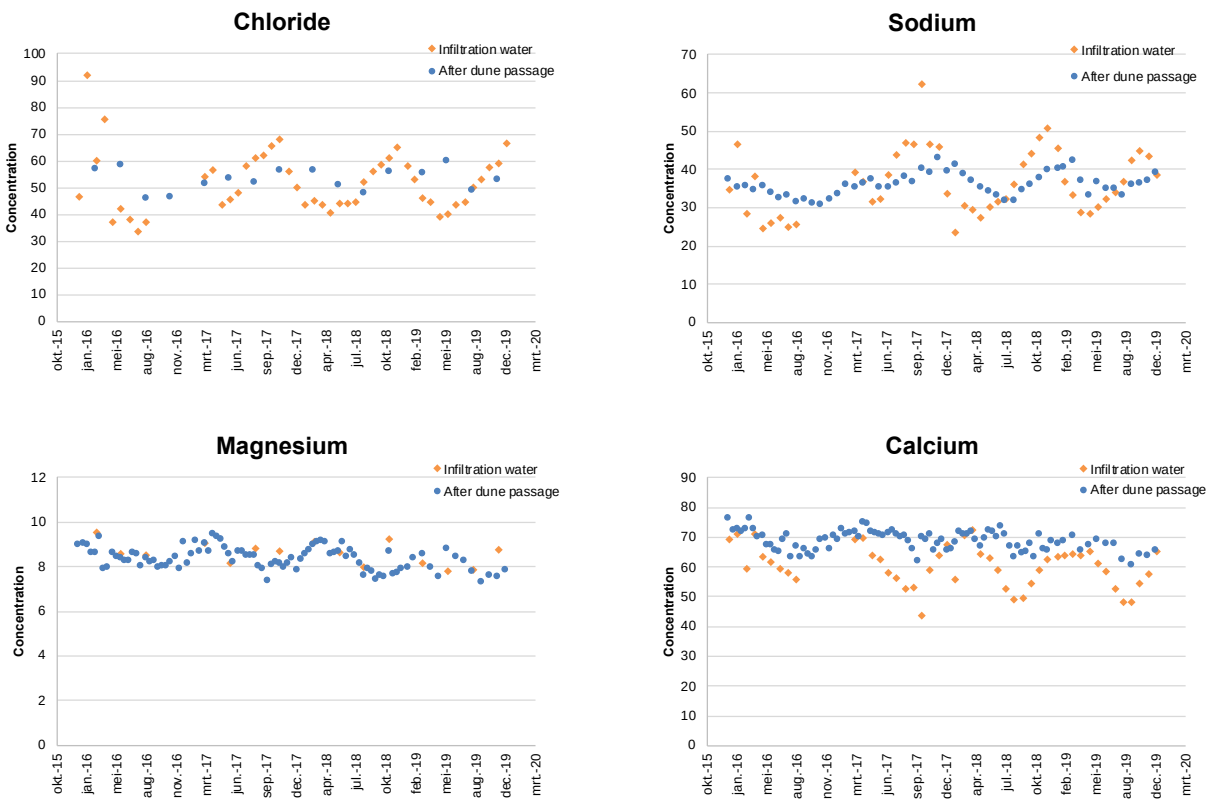

Figure 23. Different ion concentrations in infiltration water originating from the Meuse and in the abstracted water after dune passage. Data from Het Waterlaboratorium obtained by Dunea.

To obtain an all-year-round Cl^- concentration below 100 mgL^{-1}, it was calculated that in summer 75% (9330 m^3h^{-1}) and in winter 50% (6210 m^3h^{-1}) of Meuse water has to be mixed with the dNF40 permeate of 3105 m^3h^{-1}. Yearly, 95.2 million m^3 of infiltration water could be produced, which complies with the expected required total production capacity of 92 million m^3y^{-1} in 2040 (Zwolsman, 2019). At the same time, the load on the current pretreatment system is reduced with 11% in summer and even 41% in winter. When the dNF40 plant is built at Katwijk, the permeate still has to be transported to Scheveningen and Monster. In Table 10, the expected compositions of the mixed infiltration water in summer (75% Meuse, 25% dNF) and winter (50% Meuse, 50% dNF) time are shown. The hardness after abstraction is about 2.23 $mmolL^{-1}$, which is relatively high. Although the drinking water standards are met, softening is still required to comply with Dunea standards for the supply of soft water (<1.43 $mmolL^{-1}$). However, the predicted Mg^{2+} and Ca^{2+} retentions by the projection tool for the dNF40 plant were lower than the retentions obtained in the lab-scale experiments. When the same retention behavior is shown in a full-scale operating plant, the mixed water would have a lower hardness and as a possible result less softening has to be applied in the posttreatment, saving energy, materials and costs. Moreover, compared to the scenario using side stream RO (section 5.3.1), a smaller and less saltier concentrate stream will be produced in this scenario.

Table 10. Concentrations in mgL^{-1} of various ions in two mixing scenarios together with the expected Ca^{2+} concentration and hardness in $mmolL^{-1}$ after dune passage.

	Cl^-	Na^+	Mg^{2+}	Ca^{2+} in	Ca^{2+} out	Hardness
75% Meuse, 25% dNF	98	64.5	11.5	60	70	2.23
50% Meuse, 50% dNF	95	62	13.5	57	67	2.24

6
Conclusion

There is an urgent demand to remove OMPs from our drinking water sources, and due to the increasing salinity of surface waters in coastal regions, salt removal has also become an issue in the production of drinking water. In this study, the performance of the hollow fiber LbL dNF40 membrane was assessed. The objective was to investigate the removal of salts and OMPs from synthetic surface water and real lake water in order to make it suitable for dune infiltration water.

The LbL dN40 membrane had a pure water permeability of 5.8 $Lm^{-2}h^{-1}bar^{-1}$, which is lower than of flat-sheet NF membranes due to the incorporation of PEMs. The MWCO was found to be as low as approximately 200 Da, indicating that 90% of the solutes with a molecular mass of 200 Da or higher is retained. The radius of the pores was estimated to be 0.68 nm.

The aim of this study was to research the influence of several operational parameters on the retention of ions in a surface water matrix. With SW, the retention of Cl^- decreased with increasing initial Cl^- concentration, from 21.4% with initially ~120 mgL^{-1} to 16.2% with initially ~400 mgL^{-1}. Cross-flow velocity showed to have no significant effect on ion retention in SW in general as only negligible differences in retention were observed at different velocities in the range of 0.2-1.0 ms^{-1}. Lower cross-flow velocities – which are desirable as less energy is consumed – should be possible with the dNF40 membrane due to their high resistance to fouling, which was observed during the experiments.

As the average Cl^- concentration in the VM was below 150 mgL^{-1} over the past 4 years, the measured concentration of ~235 mgL^{-1} was much higher than expected. However, the average concentration is expected to rise in the future and should thus be considered. Increasing the permeate flux did not affect the retention of SO_4^{2-}, which was retained with 95-96% for SW and 98% for VM water at all applied fluxes from 11-28 Lm^2h^{-1}. The retentions of Cl^-, Na^+, Mg^{2+} and Ca^{2+} increased with increasing permeate flux for both water types.

Moreover, increasing system recovery (from 25% to 75%) improved the retentions of Cl^-, Mg^{2+} and Ca^{2+} in SW, while Na^+ retention decreased. However, the quality of the mixed permeate decreased as the feed water became more concentrated at higher recovery and thus more ions passed the membrane in absolute terms. Remarkably was the higher retention of Na^+ in VM water, which besides increased with increasing system recovery. The retention of Mg^{2+} and Ca^{2+} in VM water also increased with increasing system recovery, but was respectively 38% and 30% lower at 75% system recovery than with SW. For Cl^-, a descending trend was observed with increasing system recovery in VM water, resulting in an

overall retention of 2.4%. The mixed synthetic permeate contained 167 mgL^{-1} of Cl^-, whereas the permeate of the VM still contained 229 mgL^{-1}, which is too high for dune infiltration water for Dunea.

Multivalent ions were retained better than monovalent ions in all cases. SO_4^{2-} was retained better than Mg^{2+} and Ca^{2+} due to the strong electrostatic interactions between the divalent anion and the negatively charged membrane. The retention order in SW was $SO_4^{2-} > Mg^{2+} > Ca^{2+} > Cl^- > Na^+$. The same order could be observed in VM water for the measured divalent ions, whereas Na^+ retention was higher than Cl^- retention.

The second aim of this study was to assess the performance of the dNF40 membrane towards OMPs, and to gain more insight into the removal mechanism of the LbL structured membrane. The average retention of 20 selected OMPs was 89% for SW and 79% for VM water. Most pharmaceuticals with a molecular weight above the MWCO showed excellent removal, except for the neutral hydrochlorothiazide. Despite its low molecular weight, outstanding removal of the negatively charged gabapentin was obtained, indicating that it was rejected due to electrostatic interactions between the pharmaceutical and the negatively charged membrane.

Overall, negatively charged pharmaceuticals were retained best (97.2% for SW compared to 94.7% for VM), followed by positively charged compounds (92.0% for SW versus 79.3% for VM). The high retention of the charged compounds could be explained by the LbL structure of the membrane. The terminal polyanion layer caused highest retention for negatively charged compounds. However, underlying polycation layers probably promoted the repulsion of positively charged OMPs and hence higher rejections were observed for positively charged OMPs than with traditional flat-sheet NF membranes. Neutral pharmaceuticals were retained less (72.6% for SW compared to 56.5% for VM). A possible explanation was given for the higher retention difference between SW and VM water for positively charged OMPs with regard to the presence of NOM in VM water. NOM could have adsorbed onto the polycation, causing neutralization of the charged layer or even an increase in negative charge, leading to a higher passage of positively charged OMPs. However, more research needs to be performed to truly explain this phenomenon.

A conceptual design of a full-scale dNF40 plant was presented, where 32 million m^3y^{-1} can be treated. As for the purpose of Dunea not sufficient Cl^- is removed at higher system recoveries, four possible solutions were provided. The most interesting scenario seemed to be the mixing scenario with pretreated Meuse water, where the VM would also become a source for Scheveningen and Monster, thereby reducing the demand of the current pretreatment in Bergambacht and the pressure on the on the transportation pipes.

7
Recommendations

Based on the results obtained in this research, some questions were answered while several new questions arose that remained unanswered. The recommendations for further research are mentioned in this section.

1. Temperature and pH were kept constant in this study. However, both parameters can influence retention as they affect the passage of solutes and water molecules through the membrane. For example, temperature affects salt diffusion coefficients and water viscosity, while pH influences the charge of the membrane; at low pH, the zeta potential is expected to turn more positive due to polarization of cations at the membrane surface. In further research these parameters could be varied to obtain a better understanding of their influence on ion and OMP retention.

2. Retention is very dependent on the water matrix (Sanches et al., 2012). This was partially shown by the performed experiments, in which it became clear that concentration and also the presence of NOM can significantly influence retention values. As the water composition of surface water varies throughout the year, it is recommended to conduct experiments with real surface water over a longer period. These experiments should be executed on pilot scale to determine treatment conditions that should be incorporated in a full-scale plant.

3. The differences in cation retention between SW and real lake water could not be fully explained in this study. More extensive research with single and double salt solutions have to be executed to provide insight in the 'competing phenomena among mineral ions' (Wang et al., 2018). Also, varying with NOM concentration can potentially lead to a better insight in the mechanism behind cation retention, as the hypothesis is that the negatively charged NOM bonds with the polycation layers, thereby reducing cation repulsion caused by these layers.

4. Positively charged OMPs were better retained with the LbL dNF40 membrane than with flat sheet NF membranes. Further study should for instance focus on the electrical potential of the LbL membrane to obtain a better comprehension of the rejection mechanism behind the PEMs.

5. The retention values of OMPs mentioned in this study are based on single pass with low recovery. Because much higher recoveries are applied in drinking water treatment, the OMP retention should also be studied at higher system recovery values. For flat-sheet NF it is known

that higher system recoveries result in a decrease of retention (Verliefde et al., 2007b; Verliefde et al., 2009b).

6. Furthermore, the influence of salts on the retention of OMPs would be an interesting topic for further research as charged particles can interfere with their retention.

7. Dune passage of the produced infiltration water removes pathogenic microorganisms to a high extend so their removal by the dNF40 membrane was no topic of interest in this research. However, the disinfection capacity is important for many other applications in drinking water treatment. Besides, a focus on pathogen removal could provide useful insights that contribute to a more complete understanding of the removal mechanisms of LbL membranes.

8. The dNF process generates a concentrate stream which is not highly saline but still needs to be discharged. Future research can be focused more on the disposal and perhaps also treatment of this residual stream.

9. The efficiency of a dNF system can still be improved by optimizing operational parameters such as cross-flow velocity, applied flux and recovery as they all influence energy consumption. In addition, a detailed cost comparison with the current pretreatment of Dunea, including transportation costs and footprint of the plant, could indicate if it is beneficial to implement the dNF membranes in the pretreatment of Katwijk.

Bibliography

Abtahi, S. M., Ilyas, S., Cassan, C. J., Albasi, C., & De Vos, W. M. (2018). Micropollutants removal from secondary-treated municipal wastewater using weak polyelectrolyte multilayer based nanofiltration membranes. *Journal of membrane science*, *548*, 654-666.

Acero, J. L., Benitez, F. J., Teva, F., & Leal, A. I. (2010). Retention of emerging micropollutants from UP water and a municipal secondary effluent by ultrafiltration and nanofiltration. *Chemical Engineering Journal*, *163*(3), 264-272.

Albergamo, V., Blankert, B., Cornelissen, E. R., Hofs, B., Knibbe, W. J., van der Meer, W., & de Voogt, P. (2019). Removal of polar organic micropollutants by pilot-scale reverse osmosis drinking water treatment. *Water research*, *148*, 535-545.

Altena, L.P. van. Bedrijfsnormen van Dunea voor het te infiltreren water 2017-2021, oktober 2017.

Amiad. (2020). Sigma Pro Series. https://amiad.com/wp-content/uploads/2020/08/Sigma-Pro-EN-Ind.pdf

Arun, A. (2019). Direct Nanofiltration of Surface Water: Investigating the fouling and rejection performance of Low MWCO Hollow fiber Nanofiltration Membranes. MSc thesis, TU Delft.

Bandini, S., Drei, J., & Vezzani, D. (2005). The role of pH and concentration on the ion rejection in polyamide nanofiltration membranes. *Journal of membrane science*, *264*(1-2), 65-74.

Beekman, M., Zweers, P., Muller, A., De Vries, W., Janssen, P., & Zeilmaker, M. (2016). Evaluation of substances used in the GenX technology by Chemours, Dordrecht. *RIVM letter report 2016-0174*.

Bellona, C., & Drewes, J. E. (2005). The role of membrane surface charge and solute physico-chemical properties in the rejection of organic acids by NF membranes. *Journal of Membrane Science*, *249*(1-2), 227-234.

Bisselink, R., de Schepper, W., Trampé, J., van den Broek, W., Pinel, I., Krutko, A., & Groot, N. (2016). Mild desalination demo pilot: New normalization approach to effectively evaluate electrodialysis reversal technology. *Water Resources and Industry*, *14*, 18-25.

Botton, S., Verliefde, A. R., Quach, N. T., & Cornelissen, E. R. (2012). Influence of biofouling on pharmaceuticals rejection in NF membrane filtration. *Water research*, *46*(18), 5848-5860.

Bourgin, M., Borowska, E., Helbing, J., Hollender, J., Kaiser, H. P., Kienle, C., ... & Von Gunten, U. (2017). Effect of operational and water quality parameters on conventional ozonation and the advanced oxidation process O3/H2O2: kinetics of micropollutant abatement, transformation product and bromate formation in a surface water. *Water research*, *122*, 234-245.

Brinke, E. te, Reurink, D. M., Achterhuis, I., de Grooth, J., & de Vos, W. M. (2020a). Asymmetric polyelectrolyte multilayer membranes with ultrathin separation layers for highly efficient micropollutant removal. *Applied Materials Today*, *18*, 100471.

Brinke, E. te, Achterhuis, I., Reurink, D. M., de Grooth, J., & de Vos, W. M. (2020b). Multiple approaches to the buildup of asymmetric polyelectrolyte multilayer membranes for efficient water purification. *ACS Applied Polymer Materials*, *2*(2), 715-724.

Bruggen, B. van der, & Vandecasteele, C. (2003). Removal of pollutants from surface water and groundwater by nanofiltration: overview of possible applications in the drinking water industry. *Environmental pollution*, *122*(3), 435-445.

Bruggen, B. van der, Hawrijk, I., Cornelissen, E., & Vandecasteele, C. (2003). Direct nanofiltration of surface water using capillary membranes: comparison with flat sheet membranes. *Separation and Purification Technology*, *31*(2), 193-201.

Brunner, A. M., Bertelkamp, C., Dingemans, M. M., Kolkman, A., Wols, B., Harmsen, D., ... & ter Laak, T. L. (2020). Integration of target analyses, non-target screening and effect-based monitoring to assess OMP related water quality changes in drinking water treatment. *Science of The Total Environment*, *705*, 135779.

Chang, E. E., Chang, Y. C., Liang, C. H., Huang, C. P., & Chiang, P. C. (2012). Identifying the rejection mechanism for nanofiltration membranes fouled by humic acid and calcium ions exemplified by acetaminophen, sulfamethoxazole, and triclosan. *Journal of hazardous materials*, *221*, 19-27.

Chen, S. S., Taylor, J. S., Mulford, L. A., & Norris, C. D. (2004). Influences of molecular weight, molecular size, flux, and recovery for aromatic pesticide removal by nanofiltration membranes. *Desalination*, *160*(2), 103-111.

Cheng, C., Yaroshchuk, A., & Bruening, M. L. (2013). Fundamentals of selective ion transport through multilayer polyelectrolyte membranes. *Langmuir*, *29*(6), 1885-1892.

Cheng, W., Liu, C., Tong, T., Epsztein, R., Sun, M., Verduzco, R., ... & Elimelech, M. (2018). Selective removal of divalent cations by polyelectrolyte multilayer nanofiltration membrane: role of polyelectrolyte charge, ion size, and ionic strength. *Journal of membrane science*, *559*, 98-106.

Costa, A. R., & De Pinho, M. N. (2006). Performance and cost estimation of nanofiltration for surface water treatment in drinking water production. *Desalination*, *196*(1-3), 55-65.

Devitt, E. C., Ducellier, F., Cote, P., & Wiesner, M. R. (1998). Effects of natural organic matter and the raw water matrix on the rejection of atrazine by pressure-driven membranes. *Water Research*, *32*(9), 2563-2568.

Epsztein, R., Shaulsky, E., Dizge, N., Warsinger, D. M., & Elimelech, M. (2018). Role of ionic charge density in donnan exclusion of monovalent anions by nanofiltration. *Environmental science & technology*, *52*(7), 4108-4116.

Gärtner, R. S., Wilhelm, F. G., Witkamp, G. J., & Wessling, M. (2005). Regeneration of mixed solvent by electrodialysis: selective removal of chloride and sulfate. *Journal of membrane science*, *250*(1-2), 113-133.

Grooth, J. de, Reurink, D. M., Ploegmakers, J., de Vos, W. M., & Nijmeijer, K. (2014). Charged micropollutant removal with hollow fiber nanofiltration membranes based on polycation/polyzwitterion/polyanion multilayers. *ACS applied materials & interfaces*, *6*(19), 17009-17017.

Grooth, J. de, Haakmeester, B., Wever, C., Potreck, J., de Vos, W. M., & Nijmeijer, K. (2015). Long term physical and chemical stability of polyelectrolyte multilayer membranes. *Journal of membrane science*, *489*, 153-159.

Hajibabania, S., Verliefde, A., McDonald, J. A., Khan, S. J., & Le-Clech, P. (2011). Fate of trace organic compounds during treatment by nanofiltration. *Journal of membrane science*, *373*(1-2), 130-139.

Henning, N., Kunkel, U., Wick, A., & Ternes, T. A. (2018). Biotransformation of gabapentin in surface water matrices under different redox conditions and the occurrence of one major TP in the aquatic environment. *Water research*, *137*, 290-300.

Hopkins, Z. R., Sun, M., DeWitt, J. C., & Knappe, D. R. (2018). Recently detected drinking water contaminants: GenX and other per-and polyfluoroalkyl ether acids. *Journal-American Water Works Association*, *110*(7), 13-28.

Houtman, C. J. (2010). Emerging contaminants in surface waters and their relevance for the production of drinking water in Europe. *Journal of Integrative Environmental Sciences*, *7*(4), 271-295.

Houtman, C. J., Kroesbergen, J., Lekkerkerker-Teunissen, K., & van der Hoek, J. P. (2014). Human health risk assessment of the mixture of pharmaceuticals in Dutch drinking water and its sources based on frequent monitoring data. *Science of the Total Environment*, *496*, 54-62.

Ilyas, S., Abtahi, S. M., Akkilic, N., Roesink, H. D. W., & de Vos, W. M. (2017). Weak polyelectrolyte multilayers as tunable separation layers for micro-pollutant removal by hollow fiber nanofiltration membranes. *Journal of membrane science*, *537*, 220-228.

Jährig, J., Vredenbregt, L., Wicke, D., Miehe, U., & Sperlich, A. (2018). Capillary nanofiltration under anoxic conditions as post-treatment after bank filtration. *Water*, *10*(11), 1599.

Knol, A. H., Lekkerkerker-Teunissen, K., Houtman, C. J., Scheideler, J., Ried, A., & Van Dijk, J. C. (2015). Conversion of organic micropollutants with limited bromate formation during the Peroxone process in drinking water treatment. *Drinking Water Engineering and Science*, *8*(2), 25.

Kimura, K., Amy, G., Drewes, J., & Watanabe, Y. (2003). Adsorption of hydrophobic compounds onto NF/RO membranes: an artifact leading to overestimation of rejection. *Journal of Membrane Science*, *221*(1-2), 89-101.

Kiriukhin, M. Y., & Collins, K. D. (2002). Dynamic hydration numbers for biologically important ions. *Biophysical chemistry*, *99*(2), 155-168.

Kraaijeveld, E., Vallendar, A., & Vis, A. (2020). Design of a pre-treatment installation for Dunea in Katwijk: Decreasing the dependency on water from the river Maas. Student report CIE4415, TU Delft.

KWR. (2020). DPWE Robuustheid uitvoering doseerproeven 2017/2018 – Resultaten van doelstofanalyses, non-target screening en bioassays. KWR 2019.040, mei 2020, herziene versie.

Lenntech. (2020). Reverse Osmosis Plants. https://www.lenntech.com/systems/reverse-osmosis/ro/rosmosis.htm.

Malaisamy, R., Talla-Nwafo, A., & Jones, K. L. (2011). Polyelectrolyte modification of nanofiltration membrane for selective removal of monovalent anions. *Separation and Purification Technology*, *77*(3), 367-374.

Marcus, Y. (1988). Ionic radii in aqueous solutions. *Chemical Reviews*, *88*(8), 1475-1498.

Menne, D., Üzüm, C., Koppelmann, A., Wong, J. E., van Foeken, C., Borre, F., ... & Wessling, M. (2016b). Regenerable polymer/ceramic hybrid nanofiltration membrane based on polyelectrolyte assembly by layer-by-layer technique. *Journal of Membrane Science*, *520*, 924-932.

Moermond, C. T. A., Smit, C. E., Van Leerdam, R. C., van der Aa, N. G. F. M., & Montforts, M. H. M. M. (2016). Geneesmiddelen en Waterkwaliteit. RIVM Briefrapport 2016–0111. https://www.rivm.nl/bibliotheek/rapporten/2016-0111.pdf

Moussa, D. T., El-Naas, M. H., Nasser, M., & Al-Marri, M. J. (2017). A comprehensive review of electrocoagulation for water treatment: Potentials and challenges. *Journal of environmental management*, *186*, 24-41.

Mulder, M. (2012). *Basic principles of membrane technology*. Springer Science & Business Media.

Nederlof, M. M., Van Paassen, J. A. M., & Jong, R. (2005). Nanofiltration concentrate disposal: experiences in The Netherlands. *Desalination*, *178*(1-3), 303-312.

Ong, S. L., Zhou, W., Song, L., & Ng, W. J. (2002). Evaluation of feed concentration effects on salt/ion transport through RO/NF membranes with the Nernst-Planck-Donnan model. *Environmental engineering science*, *19*(6), 429-439.

Reemtsma, T., Miehe, U., Duennbier, U., & Jekel, M. (2010). Polar pollutants in municipal wastewater and the water cycle: occurrence and removal of benzotriazoles. *Water research*, *44*(2), 596-604.

Reemtsma, T., Berger, U., Arp, H. P. H., Gallard, H., Knepper, T. P., Neumann, M., ... & Voogt, P. D. (2016). Mind the Gap: Persistent and Mobile Organic Compounds – Water Contaminants That Slip Through.

Reurink, D. M., Haven, J. P., Achterhuis, I., Lindhoud, S., Roesink, H. D. W., & de Vos, W. M. (2018). Annealing of Polyelectrolyte Multilayers for Control over Ion Permeation. *Advanced materials interfaces*, *5*(20), 1800651.

Reurink, D. M., Te Brinke, E., Achterhuis, I., Roesink, H. D., & De Vos, W. M. (2019). Nafion-Based Low-Hydration Polyelectrolyte Multilayer Membranes for Enhanced Water Purification. *ACS applied polymer materials*, *1*(9), 2543-2551.

Sanches, S., Penetra, A., Rodrigues, A., Ferreira, E., Cardoso, V. V., Benoliel, M. J., ... & Crespo, J. G. (2012). Nanofiltration of hormones and pesticides in different real drinking water sources. *Separation and Purification Technology*, *94*, 44-53.

Scheideler, J., Lekkerkerker-Teunissen, K., Knol, T., Ried, A., Verberk, J., & van Dijk, H. (2011). Combination of O3/H2O2 and UV for multiple barrier micropollutant treatment and bromate formation control-an economic attractive option. *Water Practice and Technology*, *6*(4).

Scheurer, M., Sacher, F., & Brauch, H. J. (2009). Occurrence of the antidiabetic drug metformin in sewage and surface waters in Germany. *Journal of environmental monitoring*, *11*(9), 1608-1613.

Scheurer, M., Michel, A., Brauch, H. J., Ruck, W., & Sacher, F. (2012). Occurrence and fate of the antidiabetic drug metformin and its metabolite guanylurea in the environment and during drinking water treatment. *Water research*, *46*(15), 4790-4802.

Schoonenberg Kegel, F., Rietman, B. M., & Verliefde, A. R. D. (2010). Reverse osmosis followed by activated carbon filtration for efficient removal of organic micropollutants from river bank filtrate. *Water Science and Technology*, *61*(10), 2603-2610.

Shang, R., Goulas, A., Tang, C. Y., de Frias Serra, X., Rietveld, L. C., & Heijman, S. G. (2017). Atmospheric pressure atomic layer deposition for tight ceramic nanofiltration membranes: synthesis and application in water purification. *Journal of Membrane Science*, *528*, 163-170.

Sjerps, R. M., Kooij, P. J., van Loon, A., & Van Wezel, A. P. (2019). Occurrence of pesticides in Dutch drinking water sources. *Chemosphere*, *235*, 510-518.

Tetko, I. V., & Bruneau, P. (2004). Application of ALOGPS to predict 1-octanol/water distribution coefficients, logP, and logD, of AstraZeneca in-house database. *Journal of pharmaceutical sciences*, *93*(12), 3103-3110.

Tsuru, T., Urairi, M., Nakao, S. I., & Kimura, S. (1991). Negative rejection of anions in the loose reverse osmosis separation of mono-and divalent ion mixtures. *Desalination*, *81*(1-3), 219-227.

Verberk, J. Q. J. C., Post, J., Van der Meer, W. G. J., & Van Dijk, J. C. (2002). Direct capillary nanofiltration for ground water and surface water treatment. *Water Science and Technology: Water Supply*, *2*(5-6), 277-283.

Verliefde, A., Cornelissen, E., Amy, G., Van der Bruggen, B., & Van Dijk, H. (2007a). Priority organic micropollutants in water sources in Flanders and the Netherlands and assessment of removal possibilities with nanofiltration. *Environmental pollution*, *146*(1), 281-289.

Verliefde, A. R., Heijman, S. G. J., Cornelissen, E. R., Amy, G., Van der Bruggen, B., & Van Dijk, J. C. (2007b). Influence of electrostatic interactions on the rejection with NF and assessment of the removal efficiency during NF/GAC treatment of pharmaceutically active compounds in surface water. *Water research*, *41*(15), 3227-3240.

Verliefde, A. R., Cornelissen, E. R., Heijman, S. G. J., Verberk, J. Q. J. C., Amy, G. L., Van der Bruggen, B., & Van Dijk, J. C. (2008). The role of electrostatic interactions on the rejection of organic solutes in aqueous solutions with nanofiltration. *Journal of Membrane Science*, *322*(1), 52-66.

Verliefde, A. R., Cornelissen, E. R., Heijman, S. G. J., Petrinic, I., Luxbacher, T., Amy, G. L., ... & Van Dijk, J. C. (2009a). Influence of membrane fouling by (pretreated) surface water on rejection of pharmaceutically active compounds (PhACs) by nanofiltration membranes. *Journal of Membrane Science*, *330*(1-2), 90-103.

Verliefde, A. R., Cornelissen, E. R., Heijman, S. G. J., Verberk, J. Q., Amy, G. L., Van der Bruggen, B., & Van Dijk, J. C. (2009b). Construction and validation of a full-scale model for rejection of organic micropollutants by NF membranes. *Journal of Membrane Science*, *339*(1-2), 10-20.

Verliefde, A. R., Cornelissen, E. R., Heijman, S. G., Hoek, E. M., Amy, G. L., Bruggen, B. V. D., & Van Dijk, J. C. (2009c). Influence of solute− membrane affinity on rejection of uncharged organic solutes by nanofiltration membranes. *Environmental science & technology*, *43*(7), 2400-2406.

Wang, L. K., Chen, J. P., Hung, Y. T., & Shammas, N. K. (Eds.). (2011). *Membrane and desalination technologies* (Vol. 13). Springer Science+ Business Media, LLC.

Wang, J., Dlamini, D. S., Mishra, A. K., Pendergast, M. T. M., Wong, M. C., Mamba, B. B., ... & Hoek, E. M. (2014). A critical review of transport through osmotic membranes. *Journal of Membrane Science*, *454*, 516-537.

Wang, Z., Xiao, K., & Wang, X. M. (2018). Role of coexistence of negative and positive membrane surface charges in electrostatic effect for salt rejection by nanofiltration. *Desalination*, *444*, 75-83.

Wezel, A. P. van, van den Hurk, F., Sjerps, R. M., Meijers, E. M., Roex, E. W., & ter Laak, T. L. (2018). Impact of industrial waste water treatment plants on Dutch surface waters and drinking water sources. *Science of the Total Environment*, *640*, 1489-1499.

Wols, B. A., Hofman-Caris, C. H. M., Harmsen, D. J. H., & Beerendonk, E. F. (2013). Degradation of 40 selected pharmaceuticals by UV/H2O2. *Water research*, *47*(15), 5876-5888.

World Health Organization (WHO) (2003). Glyphosate and AMPA in drinking-water. Background document for preparation of WHO Guidelines for drinking-water quality. Geneva, World Health Organization (WHO/SDE/WSH/03.04/97).

World Health Organization. (2010). *Hardness in drinking-water: background document for development of WHO guidelines for drinking-water quality* (No. WHO/HSE/WSH/10.01/10). World Health Organization.

World Health Organization (WHO). (2011). *Guidelines for drinking-water quality*. World Health Organization.

Xu, R., Zhou, M., Wang, H., Wang, X., & Wen, X. (2020). Influences of temperature on the retention of PPCPs by nanofiltration membranes: Experiments and modeling assessment. *Journal of Membrane Science*, *599*, 117817.

Yangali-Quintanilla, V., Sadmani, A., McConville, M., Kennedy, M., & Amy, G. (2009). Rejection of pharmaceutically active compounds and endocrine disrupting compounds by clean and fouled nanofiltration membranes. *Water Research*, *43*(9), 2349-2362.

Yangali-Quintanilla, V., Maeng, S. K., Fujioka, T., Kennedy, M., & Amy, G. (2010). Proposing nanofiltration as acceptable barrier for organic contaminants in water reuse. *Journal of Membrane Science*, *362*(1-2), 334-345.

Yen, F. C., You, S. J., & Chang, T. C. (2017). Performance of electrodialysis reversal and reverse osmosis for reclaiming wastewater from high-tech industrial parks in Taiwan: A pilot-scale study. *Journal of Environmental Management*, *187*, 393-400.

Zularisam, A. W., Ismail, A. F., & Salim, R. (2006). Behaviours of natural organic matter in membrane filtration for surface water treatment—a review. *Desalination*, *194*(1-3), 211-231.

Zwolsman, G. (2019). Bronnenstudie Dunea. Inventarisatie en beoordeling van nieuwe bronnen voor drinkwater in de toekomst.

Websites

Besluit kwaliteit drinkwater BES: https://wetten.overheid.nl/BWBR0005957/2009-12-22 (accessed on 19 October 2020).

Filtration Solutions Inc.: https://filtsol.com/main/index.php/technical-info/hollow-fiber-membranes (accessed on 8 June 2020).

Infiltratiebesluit: https://wetten.overheid.nl/BWBR0028642/2010-10-10#BijlageA (accessed on 19 October 2020)

NX Filtration: https://nxfiltration.com/products/nano/ (accessed on 15 June 2020).

Pentair X-Flow: https://xflow.pentair.com/en/products/hfw1000 (accessed on 15 June 2020).

PubChem: https://pubchem.ncbi.nlm.nih.gov (accessed on 28 October 2020).

RHDHV Kostenstandaard: https://www.kostenstandaard.nl/ (accessed on 2 December 2020).

A

Appendix: Control tests MWCO

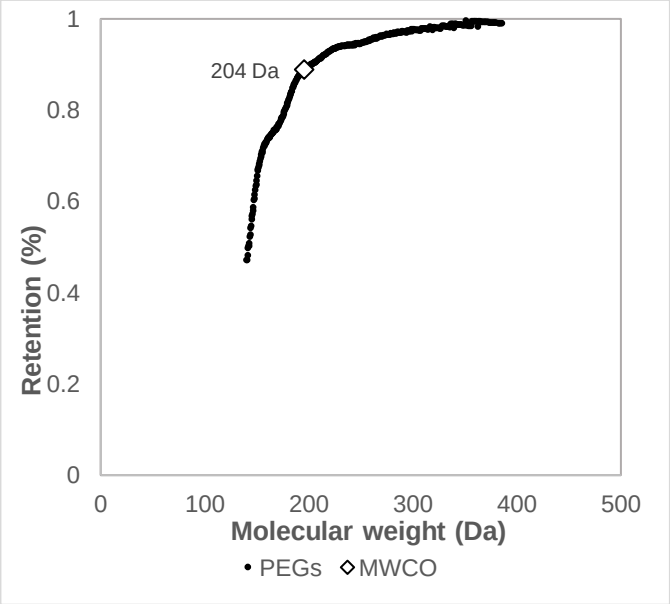

Figure 24. MWCO control test by filtration of 200 Da PEG molecules (J=18 $Lm^{-2}h^{-1}$; cfv=0.6 ms^{-1}; T=21°C).

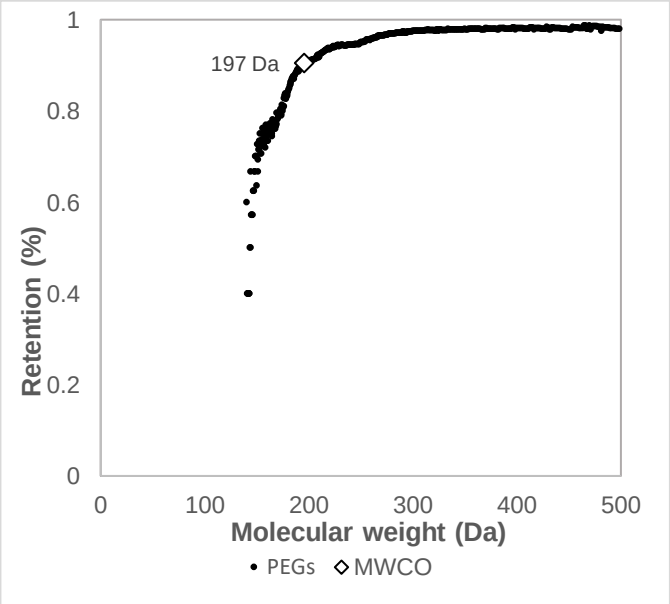

Figure 25. MWCO control test by filtration of 300 Da PEG molecules (J=18 $Lm^{-2}h^{-1}$; cfv=0.6 ms^{-1}; T=21°C).

B

Appendix: Retention OMPs

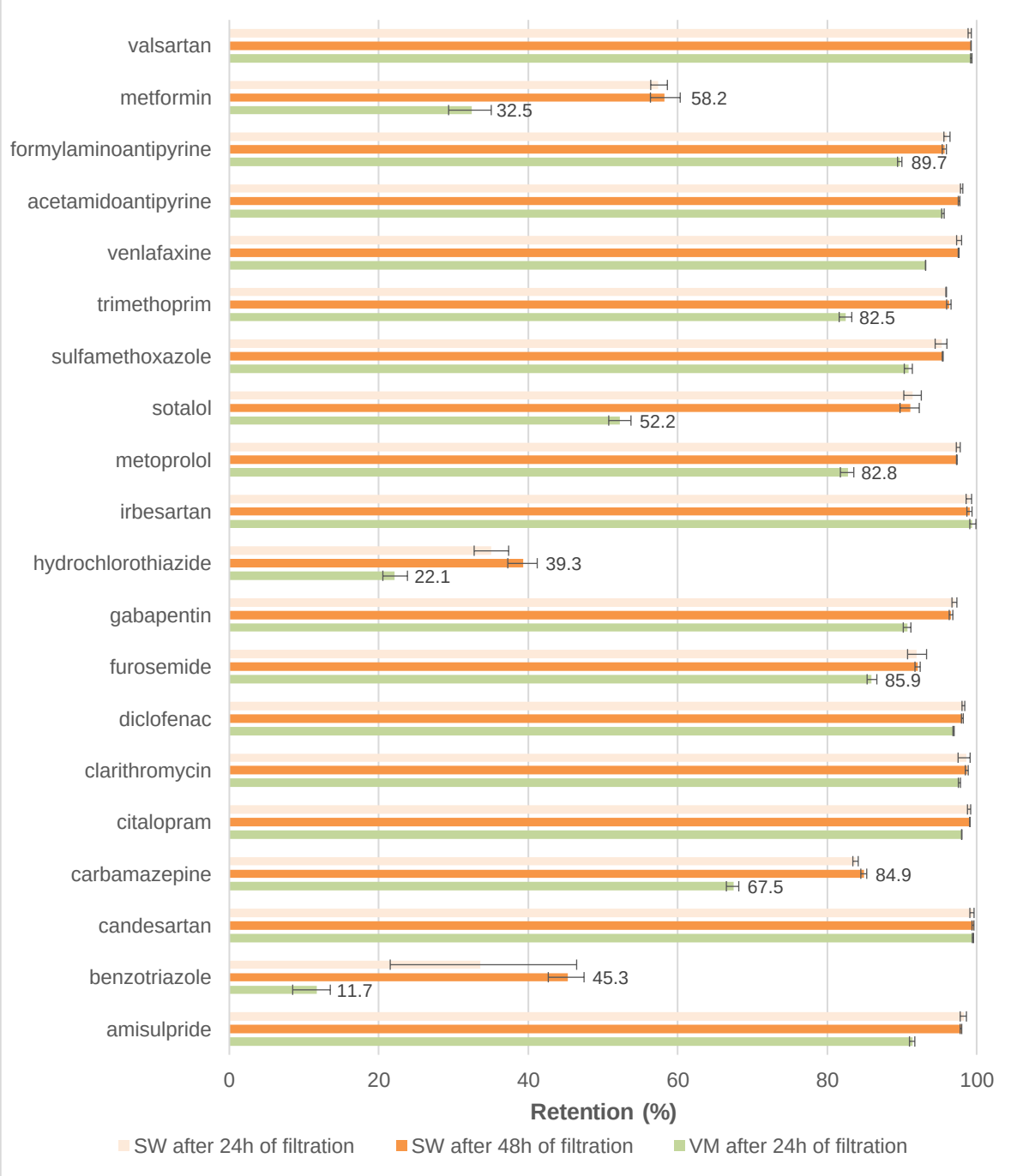

Figure 26. Retention of different OMPs during filtration of SW after 24h and 48h and VM water (cfv=0.6 ms^{-1}; T=21°C). Labels of rejection values <90% are shown.

C

Appendix: Conceptual design

Figure 27. Transport pipeline from the VM to treatment location Katwijk (left) and transport pipeline for concentrate disposal from Katwijk to the North Sea (right). Adapted from Kraaijeveld et al. (2020)

Table 111. Summer and winter water quality of the VM used for the projections.

Parameter	Winter scenario	Summer scenario	unit
pH	8.3	8.23	-
EC	920	1238	$uScm^{-1}$
Temperature	5	20	ºC
TOC	10.1	11.7	mgL^{-1}
Cl^-	143	235	mgL^{-1}
HCO_3^-	240	239	mgL^{-1}
SO_4^{2-}	72.3	90.3	mgL^{-1}
PO_4^{3-}	0.139	0.0182	mgL^{-1} P
NO_3^-	0.789	0.37	mgL^{-1} N
NH_4^+	0.0787	0.0934	mgL^{-1} N
N_{tot}	1.5	1.1	mgL^{-1} N
Na^+	93	153	mgL^{-1}
K^+	12	14.8	mgL^{-1}
Mg^{2+}	16	23.6	mgL^{-1}
Ca^{2+}	67	76.2	mgL^{-1}